Mapping IR Enhancements in Closely Interacting Spiral-Spiral Pairs. I. ISO CAM and ISO SWS Observations[1]

Cong Xu
Infrared Processing and Analysis Center, Jet Propulsion Laboratory, Caltech 100-22, Pasadena, CA 91125;
Max-Planck-Institut für Kernphysik, Postfach 103980, D69117 Heidelberg, Germany

Yu Gao, Joseph Mazzarella, Nanyao Lu
Infrared Processing and Analysis Center, Jet Propulsion Laboratory, Caltech 100-22, Pasadena, CA 91125

Jack W. Sulentic, Donovan L. Domingue
Department of Physics and Astronomy, University of Alabama, Tuscaloosa, AL 35487

ABSTRACT

Mid-infrared (MIR) imaging and spectroscopic observations are presented for a well defined sample of eight closely interacting (CLO) pairs of spiral galaxies that have overlapping disks and show enhanced far-infrared (FIR) emission. The goal is to study the star formation distribution in CLO pairs, with special emphasis on the role of 'overlap starbursts'. Observations were made with the Infrared Space Observatory (ISO) using the CAM and SWS instruments. The ISO CAM maps, tracing the MIR emission of warm dust heated by young massive stars, are compared to new ground based Hα and R-band images. We identify three possible subgroups in the sample, classified according to the star formation morphology: (1) advanced mergers (Arp 157, Arp 244 and Arp 299), (2) severely disturbed systems (Arp 81 and Arp 278), and (3) less disturbed systems (Arp 276, KPG 347 and KPG 426). Localized starbursts are detected in the overlap regions in all five pairs of subgroups (1) and (2), suggesting that they are a common property in colliding systems. Except for Arp 244, the 'overlap starburst' is usually fainter than the major nuclear starburst in CLO pairs. Star formation in 'less disturbed systems' is often distributed throughout the disks of both galaxies with no 'overlap starburst' detected in any of them. These systems also show less enhanced FIR emission, suggesting that they are in an earlier interaction stage than pairs of the other two subgroups where the direct disk collisions have probably not yet occurred.

Subject headings: galaxies: interactions – galaxies: nuclei – galaxies: starburst – infrared: galaxies – stars: formation

1. Introduction

It is well established from IRAS studies that many interacting galaxies show enhanced far-infrared (FIR) emission compared to non-interacting galaxies (Lonsdale et al. 1984; Kennicutt et al. 1987; Telesco et al. 1988). Most of the emission is due to young massive stars formed in recent starbursts, supporting the idea that galaxy-galaxy interactions can stimulate active star formation (Larson & Tinsley 1978; Rieke

[1]Based on observations made with ISO, an ESA project with instruments funded by ESA Member States and with the participation of ISAS and NASA.

et al. 1980; Condon et al. 1982; Balzano 1983; Gehrz et al. 1983; Joseph et al. 1984; Cutri & McAlary 1985); albeit, dust-obscured AGNs might be responsible for the emission in some cases (Sanders et al. 1988a; Surace & Sanders 1999; Genzel et al. 1998; Lutz et al. 1998). The most extreme FIR luminosities ($\gtrsim 10^{12}\ L_{\odot}$; H_0=75 km/s Mpc^{-1}) and highest dust temperatures are found in galaxy mergers where the identity of the component galaxies is often indeterminate (Sanders et al. 1988a; Melnick & Mirabel 1990; Mazzarella et al. 1991; Sanders & Mirabel 1996). After these ultraluminous IR galaxies (ULIRGs), violent starbursts are most likely to be found in closely interacting pairs of spiral galaxies with overlapping disks such as Arp 244 (the Antennae). These pairs dominate the FIR luminosity function between 10^{11} — $10^{12}\ L_{\odot}$ (Xu & Sulentic 1991).

There is clear evidence in the recent deep surveys carried out at: 1) optical/UV/NIR wavelengths by HST (Williams et al. 1996; Williams et al. 1998; Thompson et al. 1999), 2) MIR/FIR wavelengths by ISO (Elbaz et al. 1999; Puget et al. 1999), and 3) submm wavelengths by SCUBA (Blain et al. 1999), that much of the evolution in the history of star formation in the Universe is related to starbursts in closely interacting/merging systems. Therefore it is of great interest to understand *how* the enhanced star formation (starburst) is stimulated in these system.

The question of *how* starbursts are stimulated in interacting galaxies, leads directly to the more fundamental question of how the star formation is modulated in galaxies (Kennicutt 1989, 1998; Hunter et al. 1998; Wyse & Silk 1987; Dopita 1985). Since stars are formed from gas, an obvious necessary condition for a galaxy to be star-formation active is that it should contain significant gas. On the other hand, it appears that interacting galaxies have in general higher star formation rates (SFRs) not because they have more gas than isolated galaxies, but because the star formation rate per unit gas mass (the so called 'star formation efficiency') is much higher (Young et al. 1986, 1989; Solomon & Sage 1988; Sanders et al. 1991). As pointed out by Kennicutt (1998) in his discussion of the 'Schmidt law' (SFR$\propto \sigma_g^N$, N$\sim$ 1.4, where σ_g is the gas surface density), the higher efficiency in starbursts in interacting galaxies may simply be a consequence of their much higher gas densities (Scoville et al. 1994; Solomon et al. 1997; Gao & Solomon 1999; Bryant & Scoville 1999). Unusually high gas density, which occurs almost exclusively in the nuclei of interacting galaxies and mergers, is certainly an interaction related phenomenon. Interaction induced gas inflow is predicted by simulations and is due either to the higher gas viscosity (caused by more frequent cloud-cloud collisions in interacting galaxies: Olson & Kwan 1991a; Struck 1997), or to the torque imposed on the gas by an interaction induced stellar-bar (Barnes & Hernquist 1996).

If enhanced star formation in interacting galaxies is due to higher gas density, which has a simple physical interpretation related to the growth rate of gravitational perturbation (Kennicutt 1998), two predictions can be made:

1. Interaction induced starbursts should concentrate in the nuclear region.
2. Starbursts in interacting systems of later stages (before the majority of the gas is converted to stars) should be stronger than those in early stages, because the later the stage, the more gas will sink into the nuclei.

As far as the ULIRGs are concerned, these two predictions seem to be in good agreement with the observations (see Sanders & Mirabel 1996 for a review). All ULIRGs appear to be in or close to the final stage of the merger process (e.g. Sanders et al. 1991; Murphy et a. 1996; Clements et al. 1996; Clements and Baker 1996; Mihos & Bothun 1998). The starbursts they harbor are primarily in the nuclear regions. Mihos & Bothun (1998) noted a trend between dynamical age and $H\alpha$ concentration in the ULIRGs they

observed which is consistent with the physical scenario behind the two predictions.

Statistical studies of a large pair sample (Xu & Sulentic (1991) demonstrated that a subsample of closely interacting spiral-spiral pairs (hereafter CLO SS) with: a) separations less than a component diameter and b) showing optical signs of interaction, exhibit higher mean FIR–to–optical luminosity and FIR color ratios. This FIR excess exists not only with respect to isolated galaxies but relative to other pairs as well (see also Telesco et al. 1988; Jones & Stein 1989; Mazzarella et al. 1991). This result is again in line with prediction (2), because the small separations (normalized to the primary component diameter) of CLO SS pairs suggests that they may often be in a more advanced evolutionary state of a merger sequence compared to other SS pairs (Hwang et al. 1999). It should be noted, though, that: 1) since final coallescence usually requires several encounters between a pair of galaxies (Barnes & Hernquest 1996, 1998) and 2) since the orbital geometry of interacting systems is complicated, there is no one-to-one mapping between component separation and interaction stage. However, there is a clear tendency for the apoapsis of the orbit to decrease rapidly after the first encounter (Barnes & Hernquest 1998). This suggests that *the later the stage, the more chance for the two galaxies to remain close together.* On the other hand, the lack of one-to-one mapping between component separation and interaction stage for individual galaxy pairs (coupled with the projection effect) may be the reason for the absence of a monotonic dependence between starburst strength and separation, especially for pairs with wider separations (e.g. Fig.12 and Fig14 of Xu & Sulentic 1991; see also Keel 1993).

Contradicting prediction (1), some famous examples of the CLO SS pairs such as Arp 244 (Hummel & van del Hulst 1986; Vigroux et al. 1996; Mirabel et al. 1998) and Arp 299 (Gerhz et al. 1980; Hibbard & Yun 1998) show bright extranuclear starbursts in the overlap region, possibly due to interpenetrating collisions between components (Jog & Solomon 1992). Indeed, the simulation of Mihos et al. (1993), which modeled star formation in Arp 244 with a prescription similar to the 'Schmidt law', failed to reproduce the overlap starburst. This motivates the following two questions:

1. Are overlap and other extranuclear starbursts common in CLO SS pairs?
2. If yes, then which starburst mode is the more important in CLO SS pairs, nuclear or overlap starbursts?

One must map the star formation distribution in these systems with spatial resolutions much better than IRAS in order to answer these questions. On the other hand, since dust extinction in interacting galaxies can be very large (Gehrz et al. 1983; Kunze et al. 1996), optical star formation mapping may not provide reliable results. These considerations motivated us to map a sample of CLO SS pairs with overlapping disks using two instruments (ISO CAM and ISO PHOT) on board of the Infrared Space Observatory (Kessler et al. 1996). ISO-SWS spectroscopic observations were also made for some pairs (pointing both to the nuclei and to the overlap regions). The imaging observations provided higher angular resolutions than IRAS and orders of magnitude higher sensitivity than KAO (e.g. Bushouse et al. 1998). This paper is the first in a series that presents and analyzes the ISO observations. We report the first results of ISO CAM and ISO SWS observations, comparing them with results from new ground based Hα observations. ISO PHOT results and a more quantitative multiwavelength analysis will be presented in a following paper.

2. Observations

2.1. Sample Selection

The pair sample was selected from two catalogues:

1. Catalogue of Isolated Pairs of Galaxies in the Northern Sky (Dec.> −3 deg) by Karachentsev (1972), hereafter KPG;

2. Atlas of Peculiar Galaxies (Dec. > −27 deg) by Arp (1966).

The sample selection criteria were:

(1) spiral–spiral pairs with overlapping disks;

(2) pair component redshift difference ΔV< 500 km s^{-1};

(3) pairs showing one of the three interaction morphology classes defined in the KPG (LIN=bridges and/or tails, ATM=common halo, or DIS=distortion in one or both components);

(4) major axis diameter of the primary component D> 1′;

(5) a pair luminosity ratio $L_{fir}/L_B > 1$, where L_{fir} is the integrated IRAS FIR (82.5 μm) luminosity (Helou et al. 1988) and L_B is the combined monochromatic luminosity (νL_ν) at 4400Å estimated from the photographic magnitudes.

Criterion (1) restricts the sample to galaxy pairs with overlapping disks so that we can assess the role of overlap starbursts. This differs from the criterion used to define CLO SS pairs in Xu & Sulentic (1991) which included systems with projected separations up to one primary component diameter. Criterion (4) restricts the sample to relatively nearby pairs and insuring that the chosen sample could be resolved by ISO PHOT (beamwidth $\theta\sim$ 45″ at 60 and 100μm). The final criterion selects SS pairs with FIR/B > 2× the isolated spiral mean ($\langle L_{fir}/L_B\rangle$ = 0.5, Xu & Sulentic 1991). This is also at least 2σ above the mean L_{fir}/L_B for normal spiral galaxies studied by Corbelli et al. (1991). Our sample is biased towards FIR enhanced SS pairs in order to minimize the chance of including false CLO SS pairs (wide pairs or accordant chance alignments). It is worthwhile to mention that although FIR/B is a good measure of starburst strength (Xu & De Zotti 1989) it is affected by several factors relatively unrelated to starburst activity including B-band extinction and diffuse FIR cirrus emission. Our original sample contained ten CLO SS pairs but two (Arp 263 and KPG 536) were dropped because of poor ISO visibility parameters. Basic properties for our sample of eight CLO SS pairs are presented in Table 1.

2.2. ISO CAM Observations

The 9.7μm CAM images were obtained with the LW7 filter. They give information about the (9.7μm) silicon feature and facilitate comparisons with higher resolution ground-based (10μm) maps from the literature (e.g. Gehrz et al. 1983; Bushouse et al. 1998). The 15 μm CAM images were obtained with the LW3 filter except for the very bright source Arp 299 (IRAS 12μm flux of 3.7 Jy), where the narrower LW9 filter (centered at 15μm was used in order to avoid saturation. These maps were expected to be significantly

more sensitive than the 9.7 μm observations because the filter had a broader bandpass and because the sources were expected to be brighter at longer wavelength (less extinction and more emission). With a resolution of $\sim 10''$ these CAM images reveal structures as small as a few kpc in our sample where typical distances are $\sim 40 Mpc$ (H_0=75 km/s Mpc^{-1}). KPG 347 was a GTO target with the LW3 filter (Boselli et al. 1998). Table 2 summarizes details of the ISO CAM observations. Basic data reduction employed the CAM Interactive Analysis (CIA) software[2]. Special attention was given to the correction of transient effects using code based on the "Fouks and Schubert algorithm" developed by A. Abergel, A. Coulais, and H. Wozniak (Saclay) and provided to us by M. Sauvage (1999, private communication). This code did a significantly better job than the standard CIA algorithms.

2.3. ISO SWS Observations

We made spectroscopic observations of four emission lines (Br_β - 2.63μm; Br_α - 4.05μm; [Ne II] - 12.81μm and H_2 S(1) - 17.03μm) using ISO SWS in the grating scan mode (AOT SWS02). Observations were obtained for three pairs in our sample (marked by stars in Table 1) with three positions observed (galaxy nuclei plus overlap region) in Arp 81 and 157 and two positions (both nuclei) in Arp 278 (Table 3.1). Parameters of these observations are given in Table 3.2. The purpose of these observations was to measure star-formation rates and extinctions in different locations in the pairs. ISO SWS reductions were performed using the SWS Interactive Analysis package (IA3) developed by the international ISO SWS Consortium.

2.4. Hα Observations

Hα and R-band observations were carried out at: 1) Palomar in February 1996 using a Tek 1024×1024 CCD mounted on the 1.5m telescope giving a scale of $0\farcs62$ pixel^{-1} and 2) Calar Alto in May 1996 and August 1997 using a 2048×2048 CCD on the 2.2 m telescope giving a scale of $0\farcs33$ pixel^{-1} and/or $0\farcs53$ pixel^{-1}. Palomar narrow-band filters centered on redshifted $H\alpha$ (+ [N II]6548,6583) with FWHM $\sim$ 100 Å and adjacent continuum broad-band filter (R-band) were used. Calar Alto narrow-band (FWHM 50 – 80 Å centered on Hα) and R-band filters were also employed. The standard stars HD 84937, Landolt 104-334 (Palomar), BD +28 4211 and BD +33 2642 Calar Alto were used for photometric calibration. Standard IRAF data reduction procedures were used to reduce this data. Continuum subtracted Hα images were produced by scaling and subtracting the R frames using field stars to match the frames. Subtraction was carried out interactively until stellar residuals were minimized. Matching R band images were not obtained for all Calar Alto targets. In those cases continuum-free $H\alpha$ and [N II] emission line images were produced by subtracting the off-centered adjacent narrow-band image from the one centered on redshifted $H\alpha$ narrow-band maps, using about half dozen stars in the field for normalization. Aperture photometry was done using both elliptical and circular apertures.

---

[2]CIA is a joint development by ESA Astrophysics Division and the ISO CAM Consortium led by the ISO CAM PI, C. Cesarsky, Direction des Sciences de la Matiere, C.E.A., France.

3. Results

3.1. MIR Continuum v.s. Hα Emission

3.1.1. Individual Pair Properties

Figures 1–4 present MIR and Hα images for our sample. Three images are presented for each source. TOP PANEL: ISO CAM 15μm contours (9.7μm for KPG 347) are plotted over an optical image from the Digitized Sky Survey[3]. Contour levels are 2^n (n=1,2,3,...) times the rms noise ($\sigma_{15\mu m}$ or $\sigma_{9.7\mu m}$ for KPG 347) as given in Table 2. MIDDLE PANEL: A log grayscale image of the 15μm to 9.7μm MIR color ratio with ISO CAM 15μm contours superposed (9.7μm contours for KPG347). Contour levels are $3+3^n$ (n=0,1,2,3,...) times the rms noise of the corresponding ISO CAM image, with the range of the grayscale image varied from source to source in order to maximize the dynamic range. BOTTOM PANEL: Hα contours plotted over the R-band image. Contour levels are different for each source because of the different rms noise levels. 15 and 9.7μm flux densities are given for the sources in Table 4. The $f_{15\mu m}/f_{9.7\mu m}$ ratio depends on both small grain emission and silicate absorption in the 9.7μm band. Detailed modeling of this ratio will be presented in a future paper.

Detailed notes

Arp 299 = NGC 3690/IC 694[4] (Figures 1abc): A pair of gas-rich galaxies IC 694 (east) and NGC 3690 (west) regarded as a local example of a merger in progress (Gehrz et al. 1983; Telesco et al. 1985; Wynn-Williams et al. 1991; Casoli et al. 1999; Hibbard & Yun 1999; Gallais et al. 1999). Arp 299 is the most IR luminous system in our sample with $L_{fir} = 2.7 \times 10^{11}\ L_\odot$. Remarkably with $f_{60\mu m} = 108.9$ Jy, it is one of the brightest (60μm) extragalactic point sources in the IRAS point source catalog (Soifer et al. 1987). The component disks are in contact suggesting a relatively advanced stage of coallescence, although the nuclei are well separated and are resolved by ISO CAM. The extranuclear starburst (Source C from Gehrz et al. 1983) is about 8″ north of the NGC 3690 nucleus (Source B in Gehrz et al. 1983, the western galaxy) is only marginally resolved (seen as a plateau on the contour plot) from the latter by ISO CAM. Gallais et al. (1999) report ISO CAM CVF observations of Arp 299 which cover 48″ × 48″ with pixel size of 1.5″ × 1.5″. This can be compared to our observations (Table 2) which have a 3.8′ × 3.8′ field of view and a 3″ × 3″ pixel size. Their LW3 (15μm) map clearly resolves the overlap starburst (Source C) from the nucleus of NGC 3690.

The $f_{15\mu m}/f_{9.7\mu m}$ ratio map is generally smooth with values close to the ratio of the integrated fluxes ($f_{15\mu m}/f_{9.7\mu m} = 2$: Table 4) across most of the disks. The nucleus of IC 694 (Source A in Gehrz et al. 1983) and a few locations in the outer disk show ratios as high as $f_{15\mu m}/f_{9.7\mu m} > 10$. While high values for the ratio may have large uncertainty in the outer regions, the high ratio in the IC 694 nucleus implies a high silicate absorption which may severely depress the 9.7μm flux (see also Gehrz et al. 1983). This is consistent

[3] The Digitized Sky Survey was produced at the Space Telescope Science Institute under U.S. Government grant NAG W-2166. The images of these surveys are based on photographic data obtained using the Oschin Schmidt Telescope on Palomar Mountain and the UK Schmidt Telescope. The plates were processed into the present compressed digital form with the permission of these institutions. The complete acknowledgement can be found at http://archive.stsci.edu/dss/dss_acknowledgements.html.

[4] Confusion exists over the name of the eastern component in Arp 299. We adopt IC 694 in this paper. See Appendix in Hibbard & Yun 1998 for details.

with results of CO imaging (Sargent & Scoville 1991; Aalto et al. 1997; Casoli et al. 1999) showing that the nucleus of IC 694 has the highest surface density of molecular gas in the Arp 299 system and comparable to values found in ULIRGs (Downes & Solomon 1998). The inner part of the MIR emission region shows good correspondence with the Hα emission allowing for differences in spatial resolution (Fig. 1, Panel c). This indicates that: 1) most of the MIR emission is due to dust associated with star formation regions, as suggested by Sauvage et al. (1996) in an ISO CAM study of M51, and 2) the Hα extinction is rather smooth, consistent with the smooth $f_{15\mu m}/f_{9.7\mu m}$ ratio image. The outer envelope of the MIR emission is elongated in along PA$\sim$45° which is also the ISO CAM scan direction. The elongation is contrary to that of the Hα emission suggesting that the ISO CAM elongation is likely to be an artifact of the transient behavior in the ISO CAM detectors (Cesarsky et al. 1996). Careful transient corrections were included in our reduction of this data, but the very high surface brightness (up to $\sim$ 1 Jy/beam) in the central region of Arp 299 produce strong effects that are difficult or impossible to remove completely.

Arp 244 = NGC 4038/9 (Figures 1def): The "Antennae" are regarded as another local example of a galaxy merger (Rubin et al. 1970; Toomre & Toomre 1972; Schweizer 1978; Hummel & van der Hulst 1986; Vigroux et al. 1996; Mirabel et al. 1998; Evans et al. 1998; Whitmore et al. 1999). ISO CAM images at 6.7 and 15μm have been published (Vigroux et al. 1996; Mirabel et al. 1998). Our 9.7 and 15μm maps cover a larger area (6′ × 6′). The brightest region in this system at MIR wavelengths involves an extranuclear starburst (Source A) about 15″ northeast of the NGC 4039 nucleus (c.f. Vigroux. et al. 1996; Mirabel et al. 1998). There is an Hα peak at Source A, but much fainter than the emission from the NGC 4039 nucleus. Apparently much of the optical emission associated with Source A is extinguished by dust. More intriguingly, the FIR (60μm, 100μm and 160μm) KAO maps (Evans et al. 1998; Bushouse et al. 1998) show that the FIR peak is displaced north of Source A, at the position of a dark patch in the optical images (e.g. the HST WFPC2 images by Whitmore et al. 1999). New SCUBA maps (Haas et al. 2000) at 450 and 850μm (15″ resolution) reveal large amounts (10^{6-7} $M_\odot$) of cold dust (< 20K) in the overlap region. There are corresponding radio continuum peaks at both the MIR and FIR peaks (Hummel & van der Hulst 1986). The CO observations (Stanford et al. 1990; Gao et al. 1998; Gruendl et al. 1998) demonstrate that most of the molecular gas in this system is extended throughout the overlap region. The [C II] 158μm emission also peaks at the dark patch north of Source A (Nikola et al. 1998). All of these observations indicate that much of the star formation activity in Arp 244 is hidden by dust. Our MIR maps also show some weak emission at the beginning of the southern tail starts and a similar feature is observed in the radio continuum (Hummel & van der Hulst 1986).

The $f_{15\mu m}/f_{9.7\mu m}$ ratio map also peaks around Source A with a value of $(f_{15\mu m}/f_{9.7\mu m}) \sim 3$. Given that most of the molecular gas is found near this region (Gao et al. 1998), and very strong extinction ($A_V \simeq 70$) is found from an SWS study of MIR lines in the same region (Kunze et al. 1996), the high $(f_{15\mu m}/f_{9.7\mu m})$ level is likely due to significant silicate absorption.

In a separate ISO CAM observation (Arp 244-02, Table 2), we obtained ISO CAM LW3 images further down along the southern tail, including the end of the tail where a dwarf galaxy was found (Schweizer 1978; Mirabel et al. 1992). No MIR emission is detected in these tidal features.

Arp 157 = NGC 520a/b (Figures 2abc): This is a very complex system apparently involving two (colliding) disk galaxies, one oriented southeast-northwest (NGC 520a) and another oriented east-west (NGC 520b) (Stanford 1991; Stanford & Balcells 1990, 1991; Bernlöhr 1993ab). The collision center appears to lie near the nucleus of NGC 520b where where the MIR emission peaks. The CO emission also concentrates at this

position (Sanders et al 1988b). The H I gas shows the the kinematic signature of a rotating disk with the same orientation as NGC 520a, while the rotation center is clearly at the nucleus of NGC 520b (Hibbard & van Gorkom 1996). An interesting possibility is that the H I originally belonged to the former but has been captured by the latter (which might have an order of magnitude more mass than the former; Bernlöhr 1993b). Note also that both disks show rotation axes nearly parallel to the axis of the orbital motion (Bernlöhe 1993b), making the hypothesis for migration of the H I gas more reasonable. There is a second, much weaker peak in the MIR emission associated with the nucleus of NGC 520a, where new millimeter synthesis observations failed to detect any CO emission (Hibbard et al. 2000, private communication). The Hα map (see also Hibbard & van Gorkom 1996; and Young et al. 1988) shows very different morphology from the MIR maps which is most likely due to dust extinction of the former. Near the nucleus of NGC 520b, heavy dust lanes are visible in optical images. The ($f_{15\mu m}/f_{9.7\mu m}$) ratio, as a rough indicator of silicate absorption, also peaks there. A NIR K-band image of Arp 157 (Bushouse & Werner 1990) shows similar morphology to the MIR images, indicating that the difference between the MIR and optical/Hα morphologies is not due to different angular resolutions. This is consistent with results of Bernlöhr (1993b) whose model predicts that both NGC 520a and NGC 520b have been undergoing starbursts, with the starburst associated with NGC 520a about 2-3 10^8 years older and a factor of $\sim$ 8 fainter than the starburst associated with NGC 520b.

Arp 81 = NGC 6621/2 (Figures 2def): This system was included by Toomre (1978), along with Arp 157 and 244, in proposed sequence of mergers. A recent HST WFPC B-band image (Keel, private communication) shows that NGC 6622 (the southern galaxy) is likely to be a high inclination S0 galaxy. Hα and MIR emission from the center of NGC 6622 indicates that some star formation is occurring there but at much lower level than in the nuclear region of NGC6621. The HST image shows a star formation region between the two galaxies along with gas/dust features extend from NGC 6621 and near the center of NGC 6622. There starburst in the overlap region is seen in both Hα and MIR maps. The tidal tail is a marginal (2σ) detection on ISO CAM images. The nucleus of NGC 6622 and the overlap starburst show rather low $f_{15\mu m}/f_{9.7\mu m}$ ratios ($\sim$ 1), while the nucleus of NGC 6621 shows a higher level $f_{15\mu m}/f_{9.7\mu m}$ ($\sim$ 3). A KAO 100μm observation (Bushouse et al. 1998) detects only the NGC 6621 nucleus. Given the large beam ($\sim$ 50″) it is possible that the overlap starburst may have contributed significantly to the flux. A 1.426 GHz VLA map (Condon et al. 1996) peaks on the NGC 6621 nucleus with an extension that may be due to the overlap starburst or even emission associated with NGC 6622.

Arp 278 = NGC 7253a/b (Figures 3abc): This system looks like a more edge-on version of the famous "Taffy Galaxies" (UGC 12914/5) (Condon et al. 1993; Jarrett et al. 1999). Both galaxies are highly inclined, and much diffuse emission is observed between the two disks (as in case of "Taffy"). Arp 278 shows evidence of starbursts in both galaxies (Bernlöhr 1993a) with a possible time delay of 10-70 Myr between the components (the larger galaxy shows the younger burst). Both galaxies are detected in the radio continuum (Condon et al. 1996). MIR emission from the northwestern galaxy (NGC 7253a, the primary) peaks at the nucleus, while the peak is offset (toward the primary) in the other component. From deep optical image, the two galaxies appear to be in contact near the nucleus of the southeastern galaxy (NGC 7253b), where several Hα knots exist (Fig.3c). Given the clear link between the star formation regions in the two galaxies as shown in the Hα image, at least some of the emission in those Hα knots is likely due to overlap starburst. In connection with the Taffy Galaxy analogy (Condon et al. 1993; Jarrett et al. 1999), the components of Arp 278 may have recently undergone a face-on collision. The plumes (i.e. the diffuse emission between the two disks) may be viewed as debris from that collision. Keel (1993) suggests that NGC 7253a is undergoing a direct (prograde) encounter. Given that NGC 7253a also dominates the MIR emission of the pair (Table 4), it is likely to be the more disturbed component that is the source of

most of the debris. The ($f_{15\mu m}/f_{9.7\mu m}$) ratio map peaks at the nucleus of NGC 7253a although, in general, that ratio is not high (< 2) indicating that the overall dust extinction is less severe than in Arp 244 and 299.

Arp 276 = NGC 935/IC 1801 (Figures 3def): Neither galaxy in this pair shows evidence for strong perturbation. Both the MIR and Hα emissions extend over the galaxy disks. Most of the Hα emission in the primary comes from H II regions in the spiral structure while the nucleus shows little or no emission. This $H\alpha$ "hole" might be due to over-subtraction of the continuum or, alternatively, may indicate a high extinction in the nuclear region where the MIR emission peaks. A foreground star is projected between the two component nuclei (but not on the overlap region) making Hα measures unreliable there. Hα emission from the smaller galaxy appears more concentrated. with the nucleus contributing significantly to the total flux. Two H II regions on either side of the nucleus and perpendicular to the major axis, contribute much of the remaining Hα flux. No localized Hα or MIR feature is detected in the overlap region. Given the differences in angular resolution, the $f_{15\mu m}$ and Hα maps shows similar morphology (i.e. the emission in the primary is extended and that in the secondary is more centrally concentrated. The ($f_{15\mu m}/f_{9.7\mu m}$) ratio map is smooth with little dependence on MIR surface brightness. It is unlikely that dust extinction is high in this pair and the temperature of small grains, which are the major contributors to $f_{9.7\mu m}$ and $f_{15\mu m}$, does not depend sensitively on the radiation intensity (Désert et al. 1990).

KPG 347 = NGC 4567/8 (Figures 4abc): This pair in the Virgo cluster is known as the "Butterfly Galaxies". The $9.7\mu m$ contours are plotted in Fig. 4. The ($f_{15\mu m}/f_{9.7\mu m}$) ratio image used a $15\mu m$ map from Boselli et al (1998). The two galaxies in this system also show little morphological disturbance. A VLA H I map of the system (Cayatte et al. 1994) shows that the H I distribution of the component disks to be reasonably intact. Star formation is widespread in both galaxies and unlike the CLO SS pairs discussed above, the ($f_{15\mu m}/f_{9.7\mu m}$) ratio shows dips rather than peaks at the positions of the nuclei with high ratio plateaus in the outer disk. The reason for the variations may be different in this pair, related perhaps to heating of small grains that are responsible for MIR continuum emission. In more active pairs (e.g. Arp 299) silicate absorption is the more likely to be the major cause of variations in the flux ratio.

KPG 426 = UGC 9376a/b (Figures 4def): Deep optical image show that the component of this pair are embedded in a common envelope. Both the MIR and Hα morphologies look undistorted (symmetric). Most of the star formation in the northern galaxy is concentrated in the nucleus while that in the southern galaxy shows a nuclear and ring structure. Detailed comparison between the morphology and simulations (Toomre and Toomre 1972) suggest that the northern galaxy has undergone a retrograde encounter, while the southern galaxy a prograde but high inclination (> 30°) encounter. Similar to KPG 347, the ($f_{15\mu m}/f_{9.7\mu m}$) ratio shows dips rather than peaks in the nuclei.

3.1.2. Collective Properties

The eight systems studied in this paper provide a small but representative sample of CLO SS pairs with enhanced FIR emission. The MIR and Hα observations provide direct information about the *distribution* of star formation, which may impose new constraints on models for interaction induced star bursts. On the other hand, the uncertainties associated with small sample statistics make the following inferences suggestive rather than conclusive.

We divide our sample into three subgroups based upon the star formation morphology:

I. Advanced mergers (Arp 157, 244 and 299): The nuclei in these systems are still well separated (or they would not have been cataloged as pairs by Arp and/or Karachentsev) however both the stellar and gaseous disks are "entangled" with each other. These pairs have the least separations ($< 8kpc$) in our sample. They also show line of sight velocity differences ΔV$\leq$60 km s^{-1}, consistent with a significant dissipation of orbital angular momentum. Simulations (e.g. Mihos et al. 1993; Hibbard & Yun 1999) suggest that these pairs will merge in a few times of 10^8 years.

II. Severely disturbed systems (Arp 81 and 278): The two disks remain separated but severe tidal distortions are present. Line of sight ΔV$\sim$200 km s^{-1} for these pairs.

III. Less disturbed systems (Arp 276, KPG 347 and 426): Galaxies in these pairs show reasonably normal morphologies in both MIR and optical/Hα images. Although all three pairs are classified ATM or DIS by Karachentsev (1972), our R-band images show nearly normal (Arp 276 and KPG 347) or only weakly distorted (KPG 426) morphologies in contrast to subgroups 1) and 2). ΔV ranges from 50-150 km s^{-1} for these binary systems.

The following trends can be drawn from our observations:

1) All five CLO pairs (Arp 81, 157, 244, 278 and 299) in the first two subgroups show localized MIR and Hα emission enhancements in the overlap region. Only in Arp 244 is the overlap region starburst more luminous than the nuclei burst while in Arp 81 and 299 the overlap region starbursts are significantly fainter than the most active nucleus in the system (in Arp 157 and 278 the overlap region is close to one of the nuclei). The inference is that star formation induced by the hydrodynamic collisions of gaseous disks is a common phenomenon in closely interacting galaxy pairs. However, it is apparently seldom the dominant source of starburst emission in these systems. The nuclear starburst, driven presumably by the gravitational tidal force which induces infall of large quantities of gas into galaxy nuclei, is perhaps the major mechanism for the enhanced star formation in these galaxy pairs.

2) CLO pairs in the third subgroup show star formation that is more evenly distributed in the component galaxies. This includes both disk and nuclear activity as is observed in isolated samples at a lower average intensity level. H II emission regions in these components closely follow the spiral arms, similar to the distribution of star formation in M51 (Sauvage et al. 1996). No overlap starbursts are observed in these systems. With a caution about small sample statistics, they also show relatively low FIR/B ratios ($< L_{fir}/L_B >= 1.30 \pm 0.25$) and cool FIR colors ($< f_{60\mu m}/f_{100\mu m} >= 0.36 \pm 0.02$) compared to pairs in the first two subgroups which show $< L_{fir}/L_B >= 4.93 \pm 1.37$ and $< f_{60\mu m}/f_{100\mu m} >= 0.65 \pm 0.09$.

3.2. MIR Line Emission

The in-orbit performance of SWS over the observed wavelength regions was much lower than expected at the time our observations were planned. No Brγ or Brα features were detected while [N II] 12.81μm and H_2 S(1) 17.03μm were only detected in Arp 157. The ISO SWS results are presented in Table 6. The [N II] 12.81μm line and H_2 S(1) 17.03μm lines were only detected in the nucleus of NGC 520b (Fig. 2ab). A pointing at the overlap region in this pair also detected the [N II] 12.81μm line (Fig. 2c) but this may be contaminated by emission from the NGC 520b nucleus because of the large beam. A Brγ line (EW= 17.0$\pm$0.5 Å) was previously reported by Vanzi et al. (1998).

SWS observations of Arp 244 and 299 exist in the literature. The MIR line ratios, assuming that gas and dust are well mixed, imply rather high dust extinctions: $A_V \sim 20$ for Arp 299 and $A_V \sim 80$ for Arp 244 (Kuntz et al. 1996; Genzel et al. 1998). It is interesting to compare our new data for Arp 157 with SWS observations of related objects. The [N II] $12.81\mu m$ flux for NGC 520b is comparable to the values detected in the SWS survey of ULIRGs as well as template starburst and AGN sources (Genzel et al. 1998). A more physically meaningful comparison between sources can be made using the ratio of the [N II] $12.81\mu m$ line to total FIR flux estimated from the IRAS observations using $FIR = 1.26 \times 10^{-14}\ (2.58 f_{60\mu m} + f_{100\mu m})[W\ m^{-2}]$ (e.g., Sanders & Mirabel 1996). The ratio of $f([N\ II])/f(FIR) = 0.001$ for NGC 520b similar to the values observed in NGC 6240 and Arp 244, and about half value observed for the nuclei of Arp 299 in the more sensitive observations reported by Genzel et al. (1998). This is another direct indication that the physical conditions of active star formation in NGC 520b are similar to those observed in Arp 244 and 299, the other two sources in our first subgroup.

4. Discussion

4.1. Overlap Starbursts

What is special about the overlap region? It is the actual interface region of a disk-disk collision. An overlap starburst could then be triggered by direct collisions between giant molecular clouds (GMCs) (Noguchi 1991). At the same time this mechanism may not be very efficient because the galactic disk filling factor of GMCs is very low (> 0.01). Jog & Solomon (1992) proposed a more efficient model where collisions between H I clouds lead to the formation of a hot ionized, high-pressure remnant gas. The over-pressure due to this hot gas causes a radiative shock compression of the outer layers of existing GMCs in the overlap region. These layers become gravitationally unstable and trigger a burst of massive star formation in the initially barely stable GMCs. This model can be tested with X-ray observations of the hot remnant gas. High resolution ROSAT observations of Arp 244 (Fabbiano et al. 1997) revealed X-ray emission in the overlap region. However, given the morphology of the X-ray emission (localized, point-source like), it is more likely due to supernova remnants associated with the on-going starburst rather than a hot remnant gas which would be more diffuse. The X-ray emission and star formation associated with the ongoing collision in Stephan's Quintet (Pietsch et al. 1997; Xu et al. 1999; Sulentic et al. 2000) may be closer to this situation. Future higher resolution AXAF observations could provide more definite results.

If cloud-cloud collisions can indeed trigger star formation (Scoville et al. 1986; Olson & Kwan 1991ab) then this may be a mechanism (in addition to the gas-density dependence of star formation rate) for interaction induced star formation enhancements in general. Simulations (Olson & Kwan 1991ab; Noguchi & Ishibashi 1986; Noguchi 1988, 1991) have shown that cloud-cloud collisions are significantly enhanced throughout the disk due to the orbit-crossing of gas clouds triggered by gravitational perturbations. This may provide an interpretation for more widely distributed star formation, that shows more moderate enhancement, in "less disturbed" CLO pairs.

It is interesting to compare the overlap starbursts in Arp 299 (Source C-C' in Gehrz et al. 1983) and Arp 244 (Source A in Vigroux et al. 1996). Table 6 gives the MIR fluxes of overlap starbursts and galactic nuclei for these two systems. The overlap starburst in Arp 244 is significantly brighter than both nuclei combined! On the other hand, the overlap starburst in Arp 299 is much fainter than either of the component nuclei. One possible reason for this difference is that the two pairs are in different stages of the merging process. Arp 299 may be in a later merging stage where more gas has fallen into the galactic nuclei

powering intensive starbursts (especially in IC 694; Casoli et al. 1999). Interaction kinematics may also play a role in Arp 299 where IC 694 is undergoing a retrograde encounter (Augarde & Lequeux 1985; Hibbard & Yun 1999). This apparently allows it to retain most of its gas which is then available to the nucleus as fuel for the violent starburst. On the other hand, both disks in Arp 244 are undergoing prograde encounters (Toomre & Toomre 1972; Mihos et al. 1993), and the gas disks have suffered severe disruption (Barnes & Hernquist 1996, 1998) with much of the gas moved away from the central regions (van der Hulst 1979; Gao et al. 1998; Grundl et al. 1998). The highest gas concentration is, in fact, found in the overlap region (Stanford et al. 1990; Gao et al. 1998; Grundl et al. 1998). It is possible that such a gas distribution is unstable and transient (retardation of infall) which might be the reason why such bright overlap starbursts are rare.

4.2. 'Less Disturbed Systems'

Our third CLO SS subgroup shows a modest FIR enhancement but less structural distortion and more extended star formation. These properties are consistent with the hypothesis that they are in an earlier interaction stage than the first two subgroups. The absence of overlap starbursts in these may indicate that a disk-disk collision has not yet occurred. Although no firm conclusion can be reached about their physical separation, the calculation of Xu & Sulentic (1991, Appendix A) shows that components in most close pairs are physically proximate (physical separation $\leq$ diameter of the primary). Examination of component morphologies in KPG 426, the pair with components most clearly separated in our sample, and consideration of simulations (e.g. Toomre & Toomre 1972), suggest that the components are well separated. There is, at the same time, evidence that 'less disturbed systems' may have unfavorable interaction geometries. Two out of three pairs in subgroup three may be undergoing either retrograde or highly inclination encounters (the situation for Arp 276 is less clear).

4.3. Variations in the Strength of Star Formation Activity

We suggest that the following sequence of sources of increasing star formation efficiency: isolated galaxies – wide pairs – closely interacting pairs – ULIRGs, may be viewed as an evolutionary sequence for mergers. Results in this paper show further that, within the population of closely interacting pairs (CLO SS), the 'less disturbed systems' may be in earlier stages of interaction and have less enhanced star formation activity compared to 'severely disturbed systems' and 'advanced mergers'.

At the same time, CLO SS pairs show a large scatter in star formation indicators such as L_{fir}/L_B and $f_{60\mu m}/f_{100\mu m}$ ratios (Xu & Sulentic 1991). Even among sources from the same subgroups in this study there is a wide range in star formation activity indicators (such as FIR/B). Arp 244, one of the 'advance mergers', shows FIR/B lower than the 'less disturbed systems' and one of the lowest L_{fir}/M_{gas} ratios in interacting systems (Gao et al. 1998). One explanation for the large scatter in star formation indicators involves variations in galaxy gas content. Galaxies with less gas have less fuel for starbursts which is consistent with previous results (Sulentic 1989; Xu & Sulentic 1991) which found that SS pairs show higher FIR emission than normal galaxies but little FIR emission from pairs of early type galaxies (E/S0) which are gas poor. Differences in gas content between CLO SS pairs with strong and weak star formation enhancement will be an interesting area of study for future H I and CO surveys of galaxy pairs. A surprising lack of H I gas depletion was found in a statistical study of an FIR enhanced sample of E+S pairs (Zasov & Sulentic 1994).

Even within a sample of gas rich pairs significant differences in their star formation rates are found. This is true even for galaxies with the same gas surface density where the "star formation efficiency" can differ by as much as an order of magnitude (see, e.g., Fig. 2 of Solomon & Sage 1988). Much of this scatter may reflect the episodic nature of starbursts. Several physical mechanisms may contribute to this episodic behavior. Feed-back from massive star formation (such as supernovae explosions and stellar winds) may quench a burst after a few 10^7 yr (Krügel & Tutukov 1993). This effectively breaks the interaction induced star formation into pulses which is confirmed by observations: All starburst durations derived from observation (Rieke et al. 1980; Gehrz et al. 1983; Bernlöhr 1993a) are on the order of a few times 10^7 years even though interactions typically last for several 10^8 years (e.g. Hibbard & Yun 1999). When an interacting galaxy is observed in the 'off' stage, only a 'post-starburst' is seen (examples can be found in Bernlöhr 1993a). A 'post-starburst', with most of the OB stars already gone, will have a much reduced effect on star formation indicators (e.g. FIR and Hα emissions).

As demonstrated by the simulations of Noguchi (1991), the periodic orbital motion which swings the two galaxies back and forth relative to each other several times before they eventually merge, will induce sharp peaks (corresponding to the passages of periapses) in the cloud-cloud collision rate which in turn may also cause pulsational star formation (see also Olson & Kwan 1991ab).

The episodic nature of starbursts could be a key to understanding why only a single component in many pairs shows enhanced star formation (Joseph et al. 1984). Since the star formation in the members of a pair may well be unsynchronized (Bernlöhr 1993a), there is a good chance for one of them to be in the 'on' phase while the other is 'off'. At the same time there is a significant probability that both components will be 'on' (Lutz 1992; Surace et al. 1993). This suggests that the duration of the 'on' and 'off' phases must be comparable (a few 10^7 yrs).

Another reason for the scatter in star formation activity could be the interaction geometry. As shown in the pioneering work of Toomre & Toomre (1972), retrograde and high inclination encounters cause much less distortion than direct (prograde) and low inclination encounters. If, as suggested, the 'less disturbed systems' have unfavorable interaction geometries the lower star formation activity might result from this rather than from an earlier merger evolutionary stage. However the evidence that the galaxies in Arp 244 (lowest FIR/B in our sample) show prograde rotation (van der Hulst 1979) while IC 694 in Arp 299 (highest FIR/B in our sample) shows retrograde rotation (Hibbard & Yun 1999), argues against this possibility (see also Keel 1993; Lutz 1992). This is not meant to imply that orbital geometry plays no role in the star formation enhancement process. It suggests only that this role is likely to be complex. For example an unfavorable orbital geometry may preserve most of the original gas in a galaxy until a very late stage in the merger process, similar to the role played by a massive bulge in the simulation of Mihos & Hernquist (1996; see also Evans et al. 2000), making a ULIRG-like starburst more possible (see, e.g., the simulations of Noguchi 1991).

4.4. Galaxy Pairs and Mergers

Throughout this discussion we have adopted a scenario where galaxy pairs merge after a few close encounters, as implied by models (e.g. Barnes & Hernquist 1996, 1998). Recent studies on the cosmic evolution of merger rate using HST data (Wu & Keel 1998; Le Fèvre et al. 2000) also hint that the time scale of mergers is much shorter than the Hubble time. However, pair merger time scales as short as $\sim$ 1 Gyr require an explanation for the large number of isolated binary galaxies ($\sim$ 10% of all galaxies, Xu & Sulentic

1991), the majority of which must have been gravitationally bound systems for ~10 Gyr (Chatterjee 1987). They must also account for the rarity of candidate (early-type) merger postcursors found in the the same environments as these large pair (and compact group) populations (Sulentic & Rabaca 1994).

A possible solution for this dilemma is that today's galaxy pairs are evolved from galaxy groups. Through coalescence, within the context of hierarchical galaxy formation (White 1997), two giant galaxies observed now may be products of a long history of mergers/accretions of smaller galaxies which were formed as a bound system. One possibility is that some mixed pairs (E+S)) represent the last stages in the coallescence of a compact group (Rampazzo & Sulentic 1992). Such a picture may apply to the two giant galaxies in the Local Group (Milky Way and M31) which may represent the early stages in the formation of a CLO SS pair (e.g., Irion 2000). There is evidence that the Milky Way is still growing by accretion of smaller satellites, with the Sagittarius dwarf galaxy being the current "meal" (Buser 2000). Given the recent discoveries closely linking galaxy evolution and interactions (Williams et al. 1996; Williams et al. 1998; Thompson et al. 1999; Elbaz et al. 1999; Puget et al. 1999; Blain et al. 1999), any theory for the formation/evolution of galaxy pairs must play an integral part in the formation and evolution of galaxies in general.

5. Conclusion

We present MIR imaging and spectroscopic observations for a well defined sample of eight closely interacting pairs of spiral galaxies with overlapping disks and enhanced FIR emission. Our goal was to study the star formation distribution in these pairs with special emphasis on the importance of overlap starbursts. We identified three possible subgroups in our sample according to star formation morphology:

(1) advanced mergers;

(2) severely disturbed systems;

(3) less disturbed systems.

Overlap region starbursts are detected in all of the five pairs of subgroups (1) and (2), suggesting that they are a common property of colliding systems. On the other hand, except for Arp 244, the 'overlap starburst' is less intense than the nuclear starbursts in such pairs. Star formation pairs of subgroup (3) is often more widely distributed in the disks of both components with no evidence for overlap starbursts. These systems also show a smaller FIR enhancement, implying weaker star formation and suggesting that they may be in earlier interaction stages where direct disk-disk collisions have not yet occurred. Only one pair (Arp 157) is detected in our ISO SWS observations. The F([Ne II 12.81μm])/F(FIR) ratio in the NGC 520b component of Arp 157 is 0.1, comparable to values for other luminous infrared galaxies.

C.X. thanks Marc Sauvage for valuable assistance in reducing the ISO CAM data, and Eckard Sturm and Alberto Noriega-Crespo for helping reducing the SWS data. This work was supported by NASA grant for ISO data analysis. This research has made use of the NASA/IPAC Extragalactic Database (NED) which is operated by the Jet Propulsion Laboratory, California Institute of Technology, under contract with

the National Aeronautics and Space Administration. C.X., Y.G., J.M., and N.L. were supported by the Jet Propulsion Laboratory, California Institute of Technology, under contract with NASA.

REFERENCES

Aalto, S., Radford, S.J.E., Scoville, N.Z., Sargent, A.I. 1997, ApJ, 475, L107.

Arp, H.C. 1966, ApJS, 14, 1.

Augarde, R., Lequeux, J. 1985, A&A, 147, 273.

Balzano, V.A. 1983, ApJ, 268, 602-627 (1983).

Barnes, J., Hernquist, L. 1996, ApJ, 471, 115.

Barnes, J., Hernquist, L. 1998, ApJ, 495, 187.

Bernlöhr, K. 1993a, A&A, 268, 25.

Bernlöhr, K. 1993b, A&A, 270, 20.

Blain, A.W., Smail, I., Ivison, R.J., Kneib, J.-P. 1999, astro-ph/9908111.

Boselli, A., Lequeux, J., Sauvage, M., et al. 1998, A&A, 335, 538.

Bryant, M.B., Scoville, N.Z. 1999, AJ, 117, 2632.

Bushouse, H.A., Telesco, C.M., Werner, M.W. 1998, AJ, 115, 938.

Bushouse, H.A., Werner, M.W. 1990, ApJ, 359, 72.

Buser, R. 2000, Science, 287, 69.

Casoli, F., Willaime, M.-C., Viallefond, F., Gerin, M. 1999, A&A, 346, 663.

Cayatte, V., Kotanyi, C., Balkowski, C., van Gorkom, J.H. 1994, AJ, 107, 1003

Cesarsky, C.J., Abergel, A., Agnése, P., et al. 1996, A&A, 315, L32.

Chatterjee, T.K. 1987, Ap&SS, 135, 131.

Clements. D.L., Sutherland, W.J., McMahon, R.G., Saunders, W. 1996, MNRAS, 279, 477.

Clements. D.L., Baker, A.C. 1996, A&A, 314, L5.

Condon, J.J., Condon, M.A., Gisler, G., Puschell, J.J. 1982, ApJ, 252, 102.

Condon, J.J., Helou, G., Sanders, D.B., Soifer, B.T. 1993, AJ, 105, 1730.

Condon, J.J., Helou, G., Sanders, D.B., Soifer, B.T. 1996, ApJS, 103, 81.

Corbelli, E., Salpeter, E.E., Dickey , J.M. 1991, ApJ, 347, 49.

Cutri, R., McAlary, C.W. 1985, ApJ, 296, 90.

Désert, F.-X., Boulanger, F., Puget, J.-L. 1990, A&A, 237, 215.

Dopita, M.A. 1985, ApJ, 295, L5.

Downes, D., Solomon, P.M. 1998, ApJ, 507, 615.

Elbaz, D., Cesarsky, C.J., Fadda, D., et al. 1999, A&A, 351, L37.

Evans, R., Harper, A., Helou, G. 1998, in *Extragalactic Astronomy in Infrared*, Proceedings of the XVIIth Moriond Astrophysical Meetings, eds. G.A. Mamon, T.X. Thuan and J.T. Thanh Van; p143.

Evans, A.S., Surace, J.A., Mazzarella, J.M. 2000, ApJ, 529, L85.

Fabbiano, G., Schweizer, F., Mackie, G. 1997, ApJ, 478, 542.

Gao, Y., Gruendl, R.A., Lo, K.Y., Lee, S.-W., Hwang, C.Y. 1998, AAS, 192, #69.04.

Gao, Y., Solomon, P.M. 1999, ApJ, 512, L99.

Gallais, P., Laurent, O., Charmandaris, V., et al. 1999, Proceedings of "The Universe a seen by ISO" meeting, ESA SP-427, March 1999, p. 881.

Gehrz, R.D., Sramek, R.A., Weedman, D.W. 1983, ApJ, 267, 551.

Genzel, R., Lutz, D., Sturm, E., et al. 1998, ApJ, 495, 1998.

Goldreich, P., Tremaine, S. 1978, ApJ, 222, 850.

Gruendl R.A., Gao, Y., Lo, K.Y., Hwang, C.-Y., Lee, S.-W. 1998, AAS, 192, #69.05.

Haas, M., Klaas, U., Coulson, I. et al. 2000, A&A, submitted.

Helou, G., Khan, I.R., Malek, L., Beohmer, L. 1988, ApJS68, 151.

Hibbard, J.E., van Gorkom, J.H. 1996, AJ, 111, 655.

Hibbard, J.E., Yun, M.S. 1999, AJ, 118, 162.

Hummel, E., van der Hulst, J.M. 1986, A&A, 155, 151.

Hwang, Y.H., Lo, K.Y., Gao, Y., Gruendl, R.A., Lu, N.Y. 1999, ApJ511, L17.

Hunter, E.A., Elmegren, B.G., Baker, A.L. 1998, ApJ, 493, 595.

Irion, R. 2000, Science, 287, 62.

Jerry, T.H., Helou, G., Van Buren, D., Valjavec, E. 1999, ApJ, 118, 312.

Jones, B., Stein, W.A. 1989, AJ, 98, 1557.

Jog, C.J., Solomon, P.M. 1992, ApJ, 387, 152.

Joseph, R.D., Meikle, W.P.S., Robertson, N.A., Wright, G.S. 1984, MNRAS, 209, 111.

Karachentsev, I. 1972, Comm. Spec. Ap. Obs., USSR, 7, 1.

Keel, W.C. 1993, AJ, 106, 1771.

Kennicutt, R.C. 1989, ApJ, 344, 685.

Kennicutt, R.C. 1998, ApJ, 498, 541.

Kennicutt, R.C. Keel, W.C., van der Hulst, J.M., et al. 1987, AJ, 93, 1011.

Kessler, M.F., Steinz, J.A., Anderegg, M.E. et al. 1996, A&A, 315, L27.

Krügel, E., Tutukov, A.V. 1993, A&A, 275, 416.

Kunze, D., Rigopoulou, D., Lutz, D. et al. 1996; A&A, 315, L101.

Larson, R.B., Tinsley, B.M. 1978, ApJ, 219, 46.

Le Fèvre, O., Abraham, R., Lilly, R.S., et al. 2000, MNRAS, 331, 565.

Lonsdale, C.J., Persson, S.E., Matthews, K. 1984, ApJ, 287, 95.

Lutz, D. 1992, A&A, 259, 426.

Lutz, D., Spoon, H. W. W., Rigopoulou, D., et al. 1998, ApJ, 505, L103.

Mazzarella, J.M., Gaume, R.A., Soifer, B.T., et al. 1991, AJ, 102, 1241.

Melnick J., Mirabel, I.F. 1990, A&A, 231, 19.

Mihos, J.C. Bothun, G.D. 1998, ApJ, 500, 619.

Mihos, J.C. Bothun, G.D., Richstone, D.O. 1993, ApJ, 418, 82.

Mihos, J.C., Hernquist, L. 1996, ApJ, 464, 641.

Mirabel, I.F., Vigroux, L., Charmandaris, V., et al. 1998, A&A, 333, L1.

Mirabel, I.F., Dottori, H., Lutz, D. 1992, A&A, 256, L19.

Murphy, T., Armus, L., Mathews, K, Soifer, B.T. et al. 1996, AJ, 111, 1025.

Nikola, T., Genzel, R., Herrmann, F., et al. 1998, ApJ, 504, 749.

Noguchi, M. 1988, A&A, 203, 259.

Noguchi, M. 1991, MNRAS, 251, 360.

Noguchi, M., Ishibashi, S. 1986, MNRAS, 219, 305.

Olson, K.M., Kwan, J. 1990a, ApJ, 349, 480.

Olson, K.M., Kwan, J. 1990b, ApJ, 361, 426.

Pietsch, W., et al. A&A, 322, 89.

Puget, J-L., Lagache, G., Clements, D.L, et al. 1999, A&A345, 29.

Rampazzo, R., Sulentic, J. W. 1992, A&A, 259, 43.

Rieke, G.H., Lebofsky, M.J., Thompson, R.I., Low, F.J., Tokunaga, A.T. 1980 ApJ, 238, 24.

Rubin, V.C., Ford, W.K., D'Odorico, S. 1970, ApJ, 160, 801.

Sanders, D.B., Mirabel, I.F. 1996, ARA&A, 34, 749.

Sanders, D.B, Soifer, B.T., Elias, J.H., Madore, B.F., Matthews, K., Neugebauer, G., Scoville, N.Z. 1988a, ApJ, 325, L74.

Sanders, D.B., Scoville, N.Z., Sargent, A.I., Soifer, B.T. 1988b, ApJ, 324, L55.

Sanders, D.B., Scoville, N.Z., Soifer, B.T. 1991, ApJ, 370, 158.

Sargent, A.I., Scoville, N.Z. 1991, ApJ, 366, L1.

Sauvage, M., Blommaert, J., Boulanger, F. et al. 1996, A&A, 315, L89.

Schombert, J.M., Wallin, J.F., Struck-Marcell, C. 1990, AJ, 99, 497.

Schweizer, F. 1978, in IAU Symp. 77, p279.

Scoville, N., Hibbard, J.E., Yun, M.S., van Gorkom, J.H. 1994, in "Mass-Transfer Induced Activity in Galaxies", ed. I. Shlosman (Cambridge: Cambridge Univ. Press), p191.

Scoville, N., Sanders, D.B., Sargent, A.I., Soifer, B.T., Scott, S.L., Lo, K.Y. 1986, ApJ, 324, L55.

Soifer, B.T., Sanders, D.B., Madore, B.F., Neugebauer, G. et al. 1987, ApJ, 320, 238.

Solomon, P.M., Sage, L. 1988, ApJ, 334, 613.

Solomon, P.M., Downes, D., Radford, S.J.E., Barrett, J.W. 1997, ApJ, 478, 144.

Stanford, S.A. 1991, ApJ, 381, 409.

Stanford, S.A., Balcells, M. 1990, ApJ, 355, 59.

Stanford, S.A., Balcells, M. 1991, ApJ, 370, 118.

Stanford, S.A.., Sargent, A.I., Sanders, D.B., Scoville, N.Z. 1990, ApJ, 349, 492.

Struck, C. 1997, ApJS, 113, 269.

Sulentic, J. 1989, AJ, 98, 2066.

Sulentic, J.W. et al. 2000, in "Cosmic Evolution and Galaxy Formation", eds. J. Franco et al. (PASP), in press.

Sulentic, J.W., Rabaça, C. 1994, ApJ, 429, 531.

Surace, J.A., Mazzarella, J., Soifer, B.T., Wehrle, A.E. 1993, AJ, 105, 864.

Surace, J.A., Sanders, D.B. 1999, ApJ, 512, 162.

Telesco, C.M., Decher, R., Gatley, I. 1985, ApJ, 299, 896.

Telesco, C.M., Wolstebcroft, R., Done, C. 1988, ApJ, 329, 174.

Thomasson, M., Donner, K.J., Sundelius, B., et al. 1989, A&A, 211, 25.

Thompson, R.I., Storrie-Lombardi, L.J., Weymann, R.J., Rieke, M.J., Schneider, G., Stobie, E., Lytle, D. 1999, AJ, 117, 17.

Toomre, A. 1978, in IAU Symp. 79, p109.

Toomre, A., Toomre, J. 1972, ApJ, 178, 623.

Vanzi, L., Alonso-Herrero, A., Rieke, G.H. 1998, ApJ, 504, 93.

van der Hulst, J.M. 1979, A&A, 71, 131.

Vigroux, L., Mirabel, F., Altiéri, B. et al. 1996, A&A, 315, L93.

Young, J.S., Kleinmann, S.G., Allen, L.E. 1988, ApJ, 334, L63.

Young, J.S., Schloerb, F.P., Kenney, J.P.D., Lord, S. 1986, ApJ, 304, 443.

Young, J.S., Xie, S., Kenney, J.D.P., Rice, W.L. 1989, ApJS, 70, 699.

Wyse, R.F., Silk, J. 1987, ApJ, 339, 700.

White, S.D.M. 1997, in "The Evolution of the Universe", eds. G. Borner and S. Gottlober (New York: J. Wiley), p227.

Whitmore, B.C., Zhang, Q., Leitherer, C., et al. 1999, AJ, 118, 155.

Wynn-Williams, C.G.; Eales, S.A., Becklin, E.E., et al. 1991, ApJ, 377, 426.

Williams, S.E. et al. 1996, AJ, 112, 1335.

Williams, S.E. et al. 1998, BAAS, 193. 7501.

Wu, W., Keel, W.C. 1998, AJ, 116, 1513.

Xu, C., De Zotti, G. 1989, A&A, 225, 12.

Xu, C., Sulentic, J.W. 1991, ApJ, 374, 407.

Xu, C., Sulentic, J.W., Tuffs, R. 1999, ApJ, 512, 178.

Zasov, A., Sulentic, J.W. 1994, ApJ, 430, 179.

This preprint was prepared with the AAS LaTeX macros v4.0.

Table 1. CLO SS Pairs Sample

(1) Name	(2) R.A. (J2000)	(3) DEC. (J2000)	(4) B mag	(5) d ′ (kpc)	(6) T	(7) z km/s	(8) SEP ′ (kpc)	(9) $\frac{L_{fir}}{L_B}$	(10) $\frac{f_{60\mu m}}{f_{100\mu m}}$	(11) L_{fir} $10^{10}L_{\odot}$
Arp 157⋆:							0.65 (5.6)	4.37	0.68	4.56
NGC 520a	01h24m32.8s	+03d47m56s	12.59	1.66 (14.4)	Sc	2105				
NGC 520b	01h24m34.9s	+03d47m30s	13.55	1.14 (9.9)	Sm	2360				
Arp 276:							1.06 (16.7)	1.74	0.33	2.19
NGC 935	02h28m11.1s	+19d35m58s	13.74	1.76 (27.7)	Sb	4142				
IC 1801	02h28m12.7s	+19d35m00s	14.65	1.19 (18.7)	Sb	3970				
Arp 299:							0.38 (4.6)	9.12	0.99	26.6
NGC 3690	11h28m31.0s	+58d33m41s	12.72	1.30 (15.8)	Sc	3132				
IC 694	11h28m33.5s	+58d33m47s	12.49	1.47 (17.8)	Sc	3121				
Arp 244:							1.21 (7.7)	1.15	0.59	3.86
NGC 4038	12h01m52.8s	-18d51m54s	10.91	5.25 (33.4)	Sm	1642				
NGC 4039	12h01m55.2s	-18d53m06s	11.05	3.09 (19.7)	Sm	1641				
KPG 347:							1.30 (11.4)	1.20	0.36	3.18
NGC 4567	12h36m32.7s	+11d15m28s	12.02	2.47 (21.7)	Sb	2274				
NGC 4568	12h36m34.7s	+11d14m15s	11.99	3.50 (30.7)	Sc	2255				
KPG 426:							0.88 (26.3)	1.55	0.38	4.01
UGC 9376a	14h33m46.8s	+40d04m52s	14.80	1.35 (40.3)	Sb	7616				
UGC 9376b	14h33m48.4s	+40d05m39s	14.56	1.52 (45.3)	Sa	7764				
Arp 81⋆:							0.73 (17.9)	3.39	0.55	8.36
NGC 6621	18h12m54.7s	+68d21m49s	14.39	0.96 (23.6)	Sb	6210				
NGC 6622	18h13m00.2s	+68d21m12s	14.23	1.00 (24.6)	Sa	6466				
Arp 278⋆:							0.84 (15.0)	6.61	0.46	4.57
NGC 7253a	22h19m26.2s	+29d23m55s	15.03	1.46 (26.1)	Sm	4718				
NGC 7253b	22h19m31.3s	+29d23m25s	14.95	1.42 (25.4)	Sm	4493				

Col.(1): Names of galaxy pairs and of pair components. Pairs with ISO SWS observations (see Table 3) are marked by ⋆.

Col.(2): 2000 epoch right ascencion.

Col.(3): 2000 epoch declination.

Col.(4): Blue magnitude.

Col.(5): Major axis.

Col.(6): Hubble type.

Col.(7): Redshift.

Col.(8): Component separation.

Col.(9): FIR-to-blue luminosity ratio.

Col.(10): $\frac{f_{60\mu m}}{f_{100\mu m}}$ color ratio.

Col.(11): Integrated FIR (40–120 μm) luminosity calculated from IRAS 60μm and 100μm fluxes (Helou et al. 1988) and the mean redshift of the two components (H_0=75 km/s Mpc^{-1}).

Table 2. ISO CAM Observations of CLO SS Pairs

Name	Obs. date	Filter	λ (μm)	$\lambda/\delta\lambda$	pixel size	samp. step	M×N	map size	rms noise (1σ)
Arp 157	12.29.96	LW7	9.62	4	$3'' \times 3''$	$45'' \times 45''$	4×4	$3.8' \times 3.8'$	0.09 mJy/pix
	12.29.96	LW3	15.0	3	$3'' \times 3''$	$45'' \times 45''$	4×4	$3.8' \times 3.8'$	0.09 mJy/pix
Arp 276	8.26.96	LW7	9.62	4	$6'' \times 6''$	$60'' \times 60''$	3×3	$5.0' \times 5.0'$	0.11 mJy/pix
	8.26.96	LW3	15.0	3	$6'' \times 6''$	$60'' \times 60''$	3×3	$5.0' \times 5.0'$	0.15 mJy/pix
Arp 299	4.27.96	LW7	9.62	4	$3'' \times 3''$	$45'' \times 45''$	4×4	$3.8' \times 3.8'$	0.09 mJy/pix
	4.27.96	LW9	15.0	8	$3'' \times 3''$	$45'' \times 45''$	4×4	$3.8' \times 3.8'$	0.20 mJy/pix
Arp 244	7.16.96	LW7	9.62	4	$6'' \times 6''$	$60'' \times 60''$	4×4	$6.0' \times 6.0'$	0.21 mJy/pix
	7.16.96	LW3	15.0	3	$6'' \times 6''$	$60'' \times 60''$	4×4	$6.0' \times 6.0'$	0.17 mJy/pix
Arp 244-02	7.28.96	LW3	15.0	3	$6'' \times 6''$	$6'' \times 6''$	6×6	$3.5' \times 3.5'$	0.06 mJy/pix
KPG 347	7.4.96	LW7	9.62	4	$6'' \times 6''$	$90'' \times 90''$	3×3	$6.0' \times 6.0'$	0.47 mJy/pix
KPG 426	8.11.96	LW7	9.62	4	$6'' \times 6''$	$60'' \times 60''$	3×3	$5.0' \times 5.0'$	0.11 mJy/pix
	8.11.96	LW3	15.0	3	$6'' \times 6''$	$60'' \times 60''$	3×3	$5.0' \times 5.0'$	0.11 mJy/pix
Arp 81	8.19.96	LW7	9.62	4	$3'' \times 3''$	$45'' \times 45''$	4×4	$3.8' \times 3.8'$	0.10 mJy/pix
	8.19.96	LW3	15.0	3	$3'' \times 3''$	$45'' \times 45''$	4×4	$3.8' \times 3.8'$	0.09 mJy/pix
Arp 278	11.16.96	LW7	9.62	4	$6'' \times 6''$	$60'' \times 60''$	3×3	$5.0' \times 5.0'$	0.10 mJy/pix
	11.16.96	LW3	15.0	3	$6'' \times 6''$	$60'' \times 60''$	3×3	$5.0' \times 5.0'$	0.12 mJy/pix

Table 3.1. ISO SWS Observations of CLO SS Pairs

Name	Pointing†	R.A. (2000)	Dec. (2000)	Obs. date
Arp 157	N1	1h24m34.9s	3d 47′ 29.8″	6.24.97
	N2	1h24m32.8s	3d 47′ 55.9″	6.24.97
	OV	1h24m33.9s	3d 47′ 42.8″	6.24.97
Arp 81	N1	18h12m55.9s	68d 21′ 50.1″	4.28.97
	N2	18h13m00.1s	68d 21′ 12.3″	4.28.97
	OV	18h12m58.1s	68d 21′ 31.2″	5.29.97
Arp 278	N1	22h19m26.2s	29d 23′ 53.2″	5.9.97
	N2	22h19m28.9s	29d 23′ 11.3″	5.9.97

† Centers of ISO SWS pointings:

N1 — Nucleus of component 1 of the galaxy pair.

N2 — Nucleus of component 2 of the galaxy pair.

OV — Overlap region of the two components.

Table 3.2. Parameters of ISO SWS Observations

Line	λ (μm)	SWS-band	Aperture ($''\times''$)	Resolution ($\lambda/\delta\lambda$)	Sensitivity (3σ, Jy)
Br_β	2.63	SW-1B	14×20	1470–1750	0.057
Br_α	4.05	SW-2A	14×20	1540–2130	0.29
[Ne II]	12.81	LW-3A	14×27	1250–1760	0.80
H_2 S(1)	17.03	LW-3C	14×27	1760–2380	0.69

Table 4. ISO CAM Fluxes of CLO SS Pairs Sample

(1) Name	(2) $f_{9.7\mu}$ (mJy)	(3) $f_{15\mu}$ (mJy)
Arp 157:	358	766
NGC 520a	32	49
NGC 520b	327	715
Arp 276:	241	300
NGC 935	183	228
IC 1801	63	72
Arp 299:	1699	5977
NGC 3690	1071	3494
IC 694	550	2158
Arp 244:	1227	2124
NGC 4038	489	700
NGC 4039	738	1427
KPG 347†:	914	1269
NGC 4567†	124	252
NGC 4568†	790	1017
KPG 426:	84	110
UGC 9376a	32	41
UGC 9376b	52	66
Arp 81:	171	270
NGC 6621	129	216
NGC 6622	22	15
Arp 278:	178	253
NGC 7253a	126	200
NGC 7253b	44	49

† The $15\mu m$ data are taken from Bosselli et al. 1998.

Col.(1): Names of galaxy pairs and of pair components.

Col.(2): Flux density at $9.7\mu m$. The uncertainty is $\sim$ 15%, dominated by the calibration error.

Col.(3): Flux density at $15\mu m$. The uncertainty is $\sim$ 15%, dominated by the calibration error.

Table 5. SWS line emission of CLO SS Pairs

Name	Pointing	Flux (10^{-20} W/cm^2)			
		Br_β 2.63μm	Br_α 4.05μm	[Ne II] 12.81μm	H_2 S(1) 17.03μm
Arp 157	N1	< 2.3	< 2.2	19.3 ($\pm$1.5)	2.60 ($\pm$0.34)
	N2	< 0.6	< 2.2	< 1.4	< 1.4
	OV	< 0.6	< 2.2	4.88 ($\pm$0.96)	< 1.4
Arp 81	N1	< 0.6	< 3.0	< 1.4	< 1.4
	N2	< 2.3	< 2.2	< 0.7	< 0.5
	OV	< 0.6	< 3.0	< 1.9	< 1.2
Arp 278	N1	< 0.4	< 3.0	< 1.2	< 0.9
	N2	< 0.5	< 2.2	< 2.3	< 1.2

Table 6. ISO CAM Fluxes of Nuclear and Overlap Starburst Emission in Arp 299 and Arp 244

(1) Name	(2) R.A. (J2000)	(3) DEC. (J2000)	(4) $f_{9.7\mu}$ (mJy)	(5) $f_{15\mu}$ (mJy)
Arp 299:				
NGC 3690*	11h28m31.0s	+58d33m41s	613 (±65)	1410 (±150)
IC 694*	11h28m33.5s	+58d33m47s	221 (±25))	1044 (±110)
overlap starburst‡	11h28m31.0s	+58d33m49s	123 (±25)	471 (±70)
Arp 244:				
NGC 4038*	12h01m52.8s	-18d51m54s	74 (±10)	135 (±20)
NGC 4039*	12h01m55.2s	-18d53m06s	39 (±10)	76 (±20)
overlap starburst*	12h01m54.8s	-18d53d03s	142 (±18)	359 (±50)

* Fluxes estimated from point source extractions.

‡ Fluxes estimated by summing up the counts in a region of size$\sim$ 15″ after the source associated to the nucleus of NGC 3690 is extracted.

Fig. 1.— MIR and Hα emissions of Arp 299 and Arp 244. **Arp 299:** (a) Contours of 15μm emission on optical (DSS) image. Contour levels are 2^n (n=1,2,3,...) $\times\sigma_{15\mu m}$ ($\sigma_{15\mu m} = 22\mu Jy/arcsec^2$). Scale: $1' = 12.1$ kpc. (b) Grayscale (logarithmic scale) image of $f_{15\mu m}/f_{9.7\mu m}$ ratio, in the range of 1 (dark) and 10 (bright), overlaid with 15μm contours (levels: $3 + 3^n$ (n=0,1,2,...) $\times\sigma_{15\mu m}$). (c) Hα contours (levels: $3 + 3^n$ (n=1,2,3,...) $\times 10^{-17}$ $erg\,sec^{-1}cm^{-2}pix^{-1}$, $pix = 0.62''$) on R band images. Note that the overlap starburst (Source C in Gehrz et al. 1983) is only $\sim 8''$ above the nucleus of NGC 3690 (the western galaxy). **Arp 244:** (d) Contours of 15μm emission on optical (DSS) image. Contour levels are 2^n (n=1,2,3,...) $\times\sigma_{15\mu m}$ ($\sigma_{15\mu m} = 4.7\mu Jy/arcsec^2$). Scale: $1' = 6.4$ kpc. (e) Grayscale (logarithmic scale) image of $f_{15\mu m}/f_{9.7\mu m}$ ratio, in the range of 1 (dark) and 4 (bright), overlaid with 15μm contours (levels: $3 + 3^n$ (n=0,1,2,...) $\times\sigma_{15\mu m}$). (f) Hα contours (levels: $2 + 3^n$ (n=1,2,3,...) $\times 10^{-17}$ $erg\,sec^{-1}cm^{-2}pix^{-1}$, $pix = 0.62''$) on R band images. Note that the overlap starburst (Source A in Vigroux et al. 1996) coincides with the southern peak of the 15μm emission, while the nucleus of NGC 4039 (the southern galaxy) is $\sim 10''$ southwest of the peak.

Fig. 2.— MIR and Hα emissions of Arp 157 and Arp 81. **Arp 157:** (a) Contours of 15μm emission on optical (DSS) image. Contour levels are 2^n (n=1,2,3,...) $\times\sigma_{15\mu m}$ ($\sigma_{15\mu m} = 10\mu Jy/arcsec^2$). Scale: $1' = 8.6$ kpc. (b) Grayscale (logarithmic scale) image of $f_{15\mu m}/f_{9.7\mu m}$ ratio, in the range of 1 (dark) and 2.5 (bright), overlaid with 15μm contours (levels: $3 + 3^n$ (n=0,1,2,...) $\times\sigma_{15\mu m}$). (c) Hα contours (levels: $3 + 3^n$ (n=1,2,3,...) $\times 10^{-17}$ $erg\,sec^{-1}cm^{-2}pix^{-1}$, $pix = 0.53''$) on R band images. Note that the Hα observation was nonphotometric, so the calibration is a rough estimate. **Arp 81:** (d) Contours of 15μm emission on optical (DSS) image. Contour levels are 2^n (n=1,2,3,...) $\times\sigma_{15\mu m}$ ($\sigma_{15\mu m} = 10\mu Jy/arcsec^2$). Scale: $1' = 24.6$ kpc. (e) Grayscale (logarithmic scale) image of $f_{15\mu m}/f_{9.7\mu m}$ ratio, in the range of 1 (dark) and 3.16 (bright), overlaid with 15μm contours (levels: $3+3^n$ (n=0,1,2,...) $\times\sigma_{15\mu m}$). (f) Hα contours (levels: $1 + 3^n$ (n=1,2,3,...) $\times 10^{-17}$ $erg\,sec^{-1}cm^{-2}pix^{-1}$, $pix = 0.62''$) on R band images.

Fig. 3.— MIR and Hα emissions of Arp 278 and Arp 276. **Arp 278:** (a) Contours of 15μm emission on optical (DSS) image. Contour levels are 2^n (n=1,2,3,...) $\times\sigma_{15\mu m}$ ($\sigma_{15\mu m} = 3.3\mu Jy/arcsec^2$). Scale: $1' = 17.9$ kpc. (b) Grayscale (logarithmic scale) image of $f_{15\mu m}/f_{9.7\mu m}$ ratio, in the range of 1 (dark) and 2 (bright), overlaid with 15μm contours (levels: $3 + 3^n$ (n=0,1,2,...) $\times\sigma_{15\mu m}$). (c) Hα contours (levels: $1 + 3^n$ (n=1,2,3,...) $\times 10^{-17}$ $erg\,sec^{-1}cm^{-2}pix^{-1}$, $pix = 0.33''$) on R band images. **Arp 276:** (d) Contours of 15μm emission on optical (DSS) image. Contour levels are 2^n (n=1,2,3,...) $\times\sigma_{15\mu m}$ ($\sigma_{15\mu m} = 4.2\mu Jy/arcsec^2$). Scale: $1' = 15.7$ kpc. (e) Grayscale (logarithmic scale) image of $f_{15\mu m}/f_{9.7\mu m}$ ratio, in the range of 1 (dark) and 2 (bright), overlaid with 15μm contours (levels: $3 + 3^n$ (n=0,1,2,...) $\times\sigma_{15\mu m}$). (f) Hα contours (levels: $1+3^n$ (n=1,2,3,...) $\times 10^{-17}$ $erg\,sec^{-1}cm^{-2}pix^{-1}$, $pix = 0.53''$) on R band images. Note that the Hα observation was nonphotometric, so the calibration is a rough estimate.

Fig. 4.— MIR and Hα emissions of KPG 347 and KPG 426. **KPG 347:** (a) Contours of 9.7μm emission on optical (DSS) image. Contour levels are 2^n (n=1,2,3,...) $\times\sigma_{9.7\mu m}$ ($\sigma_{9.7\mu m} = 13\mu Jy/arcsec^2$). Scale: $1' = 8.8$ kpc. (b) Grayscale (logarithmic scale) image of $f_{15\mu m}/f_{9.7\mu m}$ ratio, in the range of 1 (dark) and 2 (bright), overlaid with 9.7μm contours (levels: $3 + 3^n$ (n=0,1,2,...) $\times\sigma_{9.7\mu m}$). (c) Hα contours (levels: $1 + 3^n$ (n=1,2,3,...) $\times 10^{-17}$ $erg\,sec^{-1}cm^{-2}pix^{-1}$, $pix = 0.33''$) on R band images. **KPG 426:**

(d) Contours of $15\mu m$ emission on optical (DSS) image. Contour levels are 2^n (n=1,2,3,...) $\times\sigma_{15\mu m}$ ($\sigma_{15\mu m} = 3.1\mu Jy/arcsec^2$). Scale: $1' = 30.0$ kpc. (e) Grayscale (logarithmic scale) image of $f_{15\mu m}/f_{9.7\mu m}$ ratio, in the range of 1 (dark) and 2 (bright), overlaid with $15\mu m$ contours (levels: $3 + 3^n$ (n=0,1,2,...) $\times\sigma_{15\mu m}$). (f) Hα contours (levels: $1+3^n$ (n=1,2,3,...) $\times 10^{-17}\ erg\ sec^{-1}cm^{-2}pix^{-1}$, $pix = 0.33''$) on R band images. Note that the Hα observation was nonphotometric, so the calibration is a rough estimate.

Fig. 5.— [NeII 12.81μm] line emission from the Arp 157-N1 region (nucleus of NGC 520b).

Fig. 6.— [H_2 S(1) 17.03μm] line emission from the Arp 157-N1 region (nucleus of NGC 520b).

Fig. 7.— [NeII 12.81μm] line emission from the Arp 157-OV region (between nuclei of NGC 520a and NGC 520b).

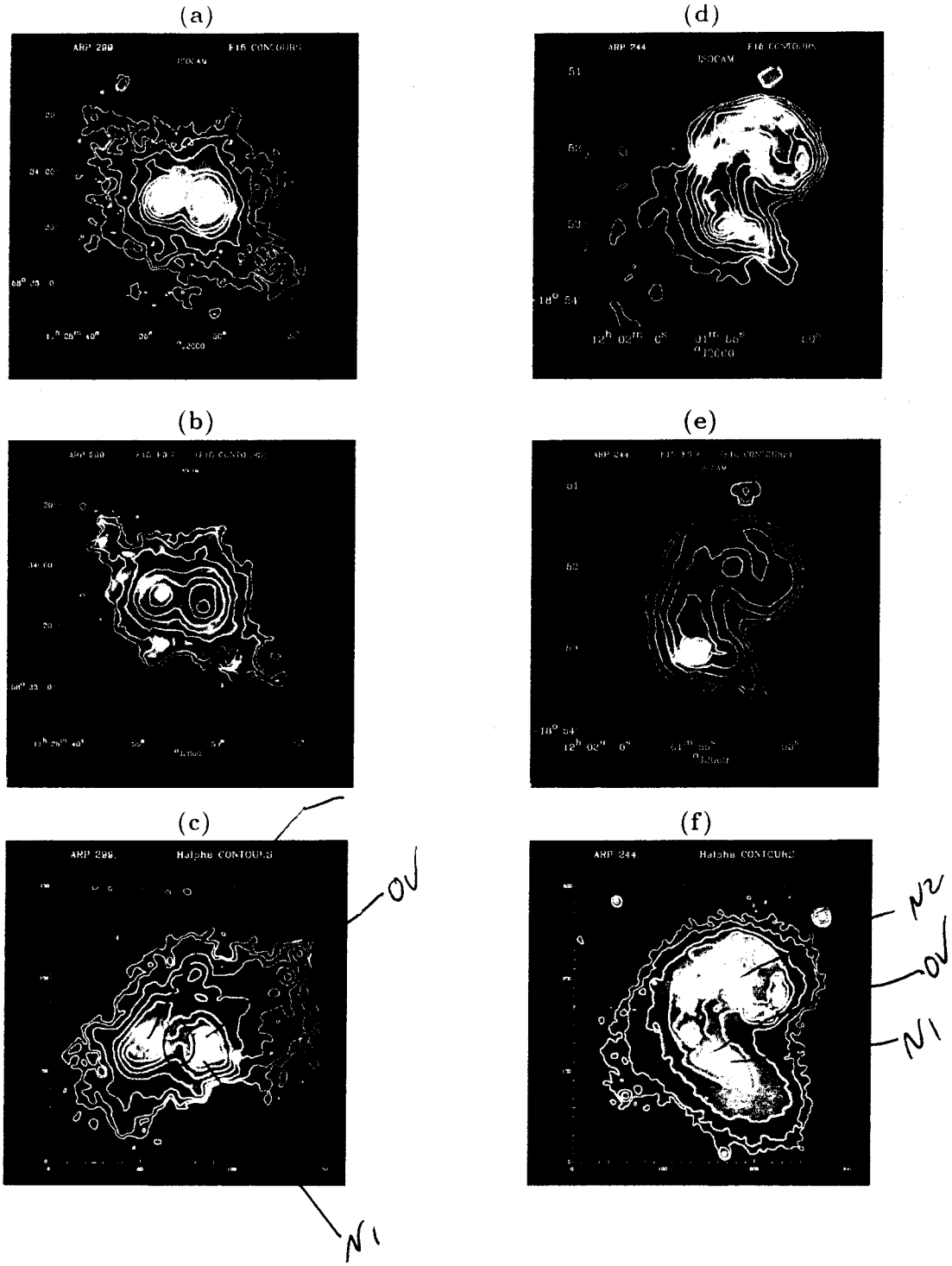
(a)
(d)
(b)
(e)
(c)
(f)
ARP 299
Halpha CONTOURS
ARP 244
Halpha CONTOURS
OV
N1
N2
OV
N1

Fig. 1.

(a)

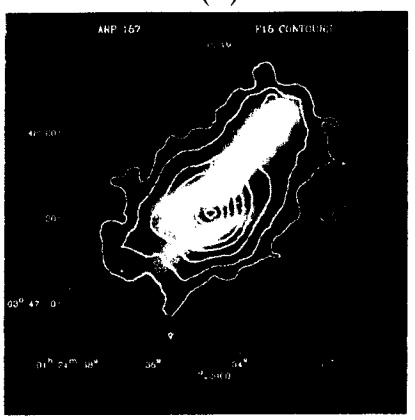
ARP 157
F16 CONTOURS

(b)

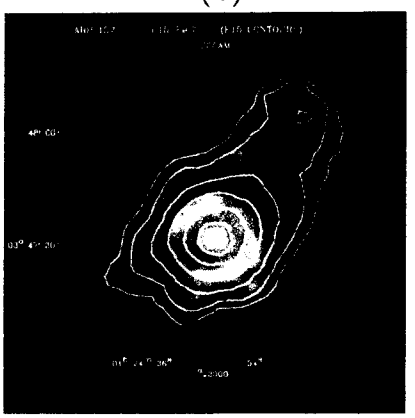

(c)

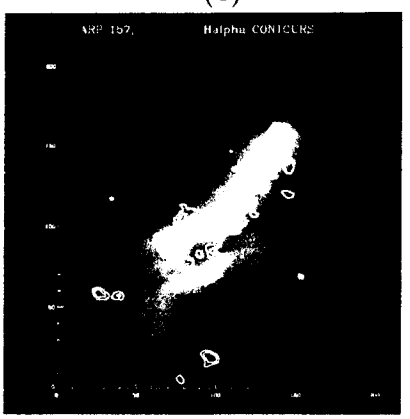
ARP 157,
Halpha CONTOURS

(d)

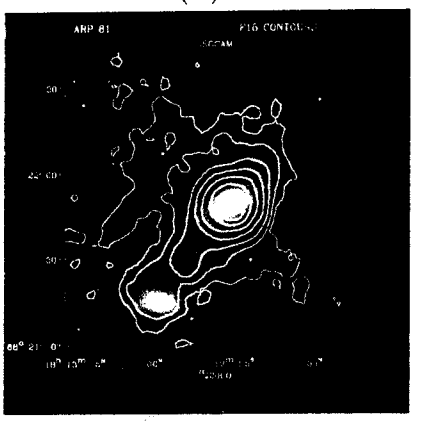
ARP 81

(e)

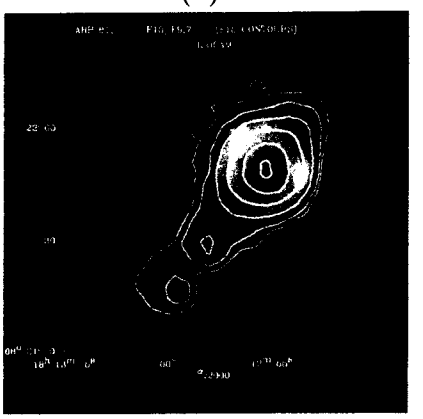

(f)

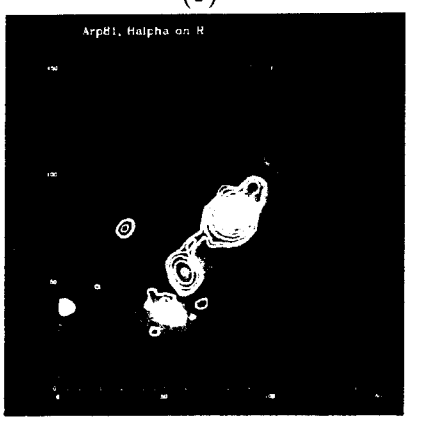
Arp81, Halpha on R

Fig. 2.

(a)

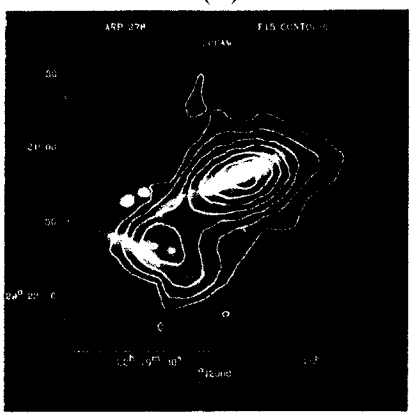

(b)

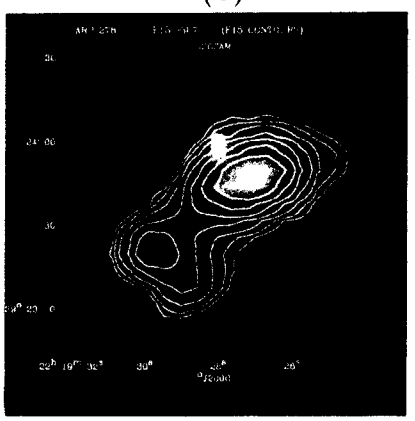

(c)

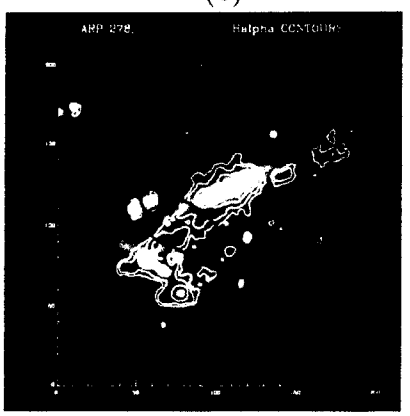

(d)

(e)

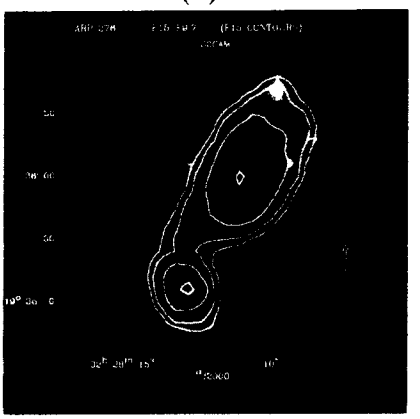

(f)

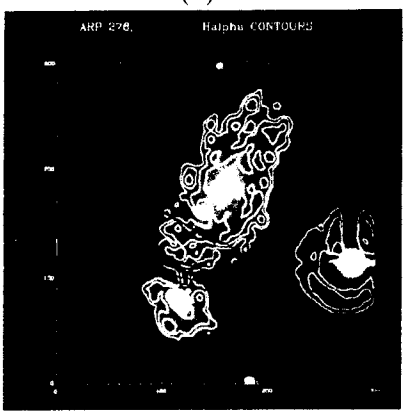

How does "bridge" of 15cm emission in Arp 27 differ from Arp 2 or others w/ "overlap" emission

Fig. 3.

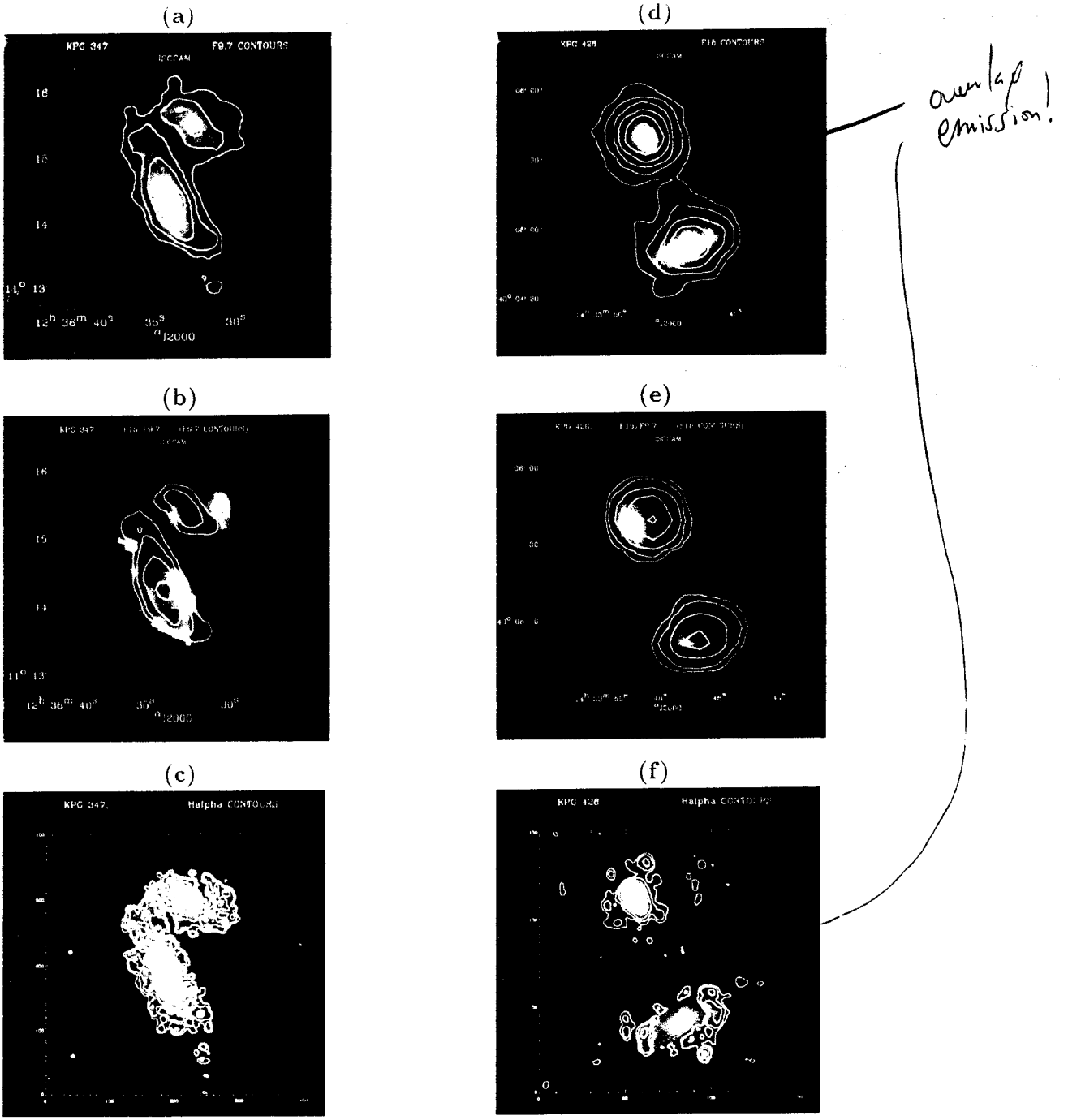
(a)
KPC 347
F9.7 CONTOURS
(b)
(c)
KPC 347.
Halpha CONTOURS
(d)
KPC 428
F16 CONTOURS
(e)
(f)
KPC 428.
Halpha CONTOURS
overlap emission!

Fig. 4.

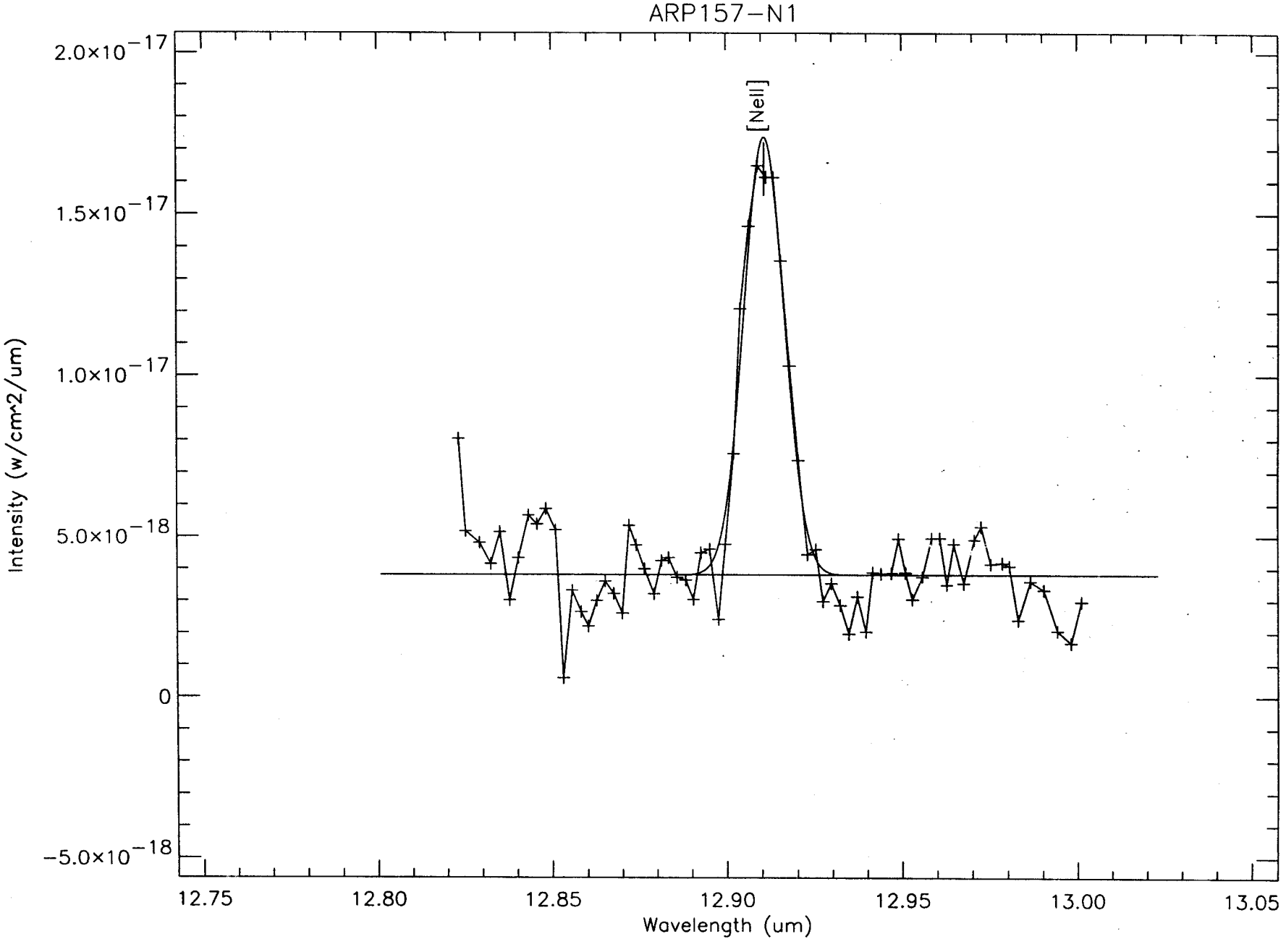
ARP157-N1
[NeII]
2.0×10^-17
1.5×10^-17
1.0×10^-17
5.0×10^-18
0
-5.0×10^-18
Intensity (w/cm^2/um)
12.75
12.80
12.85
12.90
12.95
13.00
13.05
Wavelength (um)

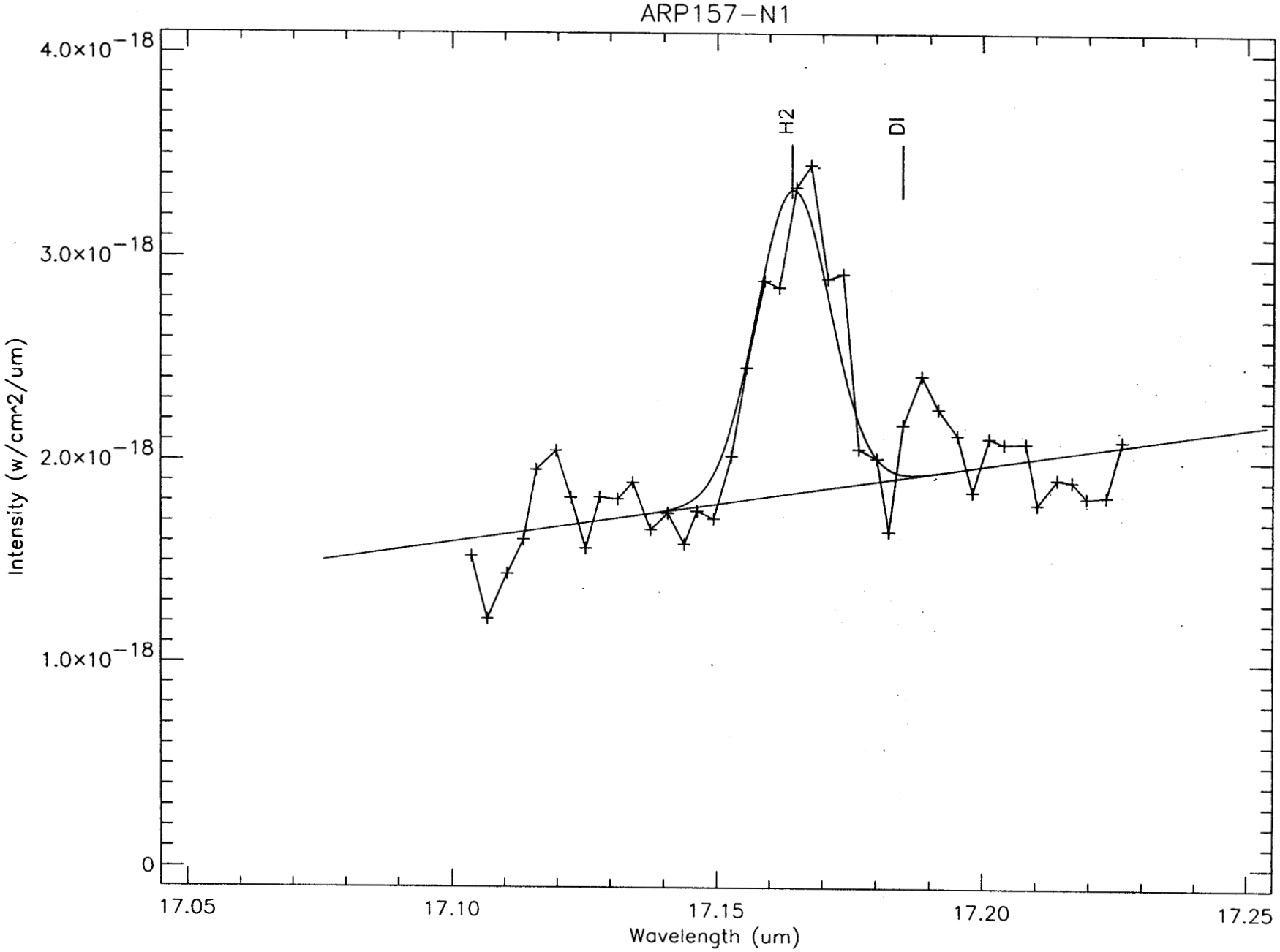
ARP157-N1
4.0×10⁻¹⁸
3.0×10⁻¹⁸
2.0×10⁻¹⁸
1.0×10⁻¹⁸
0
Intensity (w/cm^2/um)
H2
DI
17.05
17.10
17.15
17.20
17.25
Wavelength (um)

Fig. 6

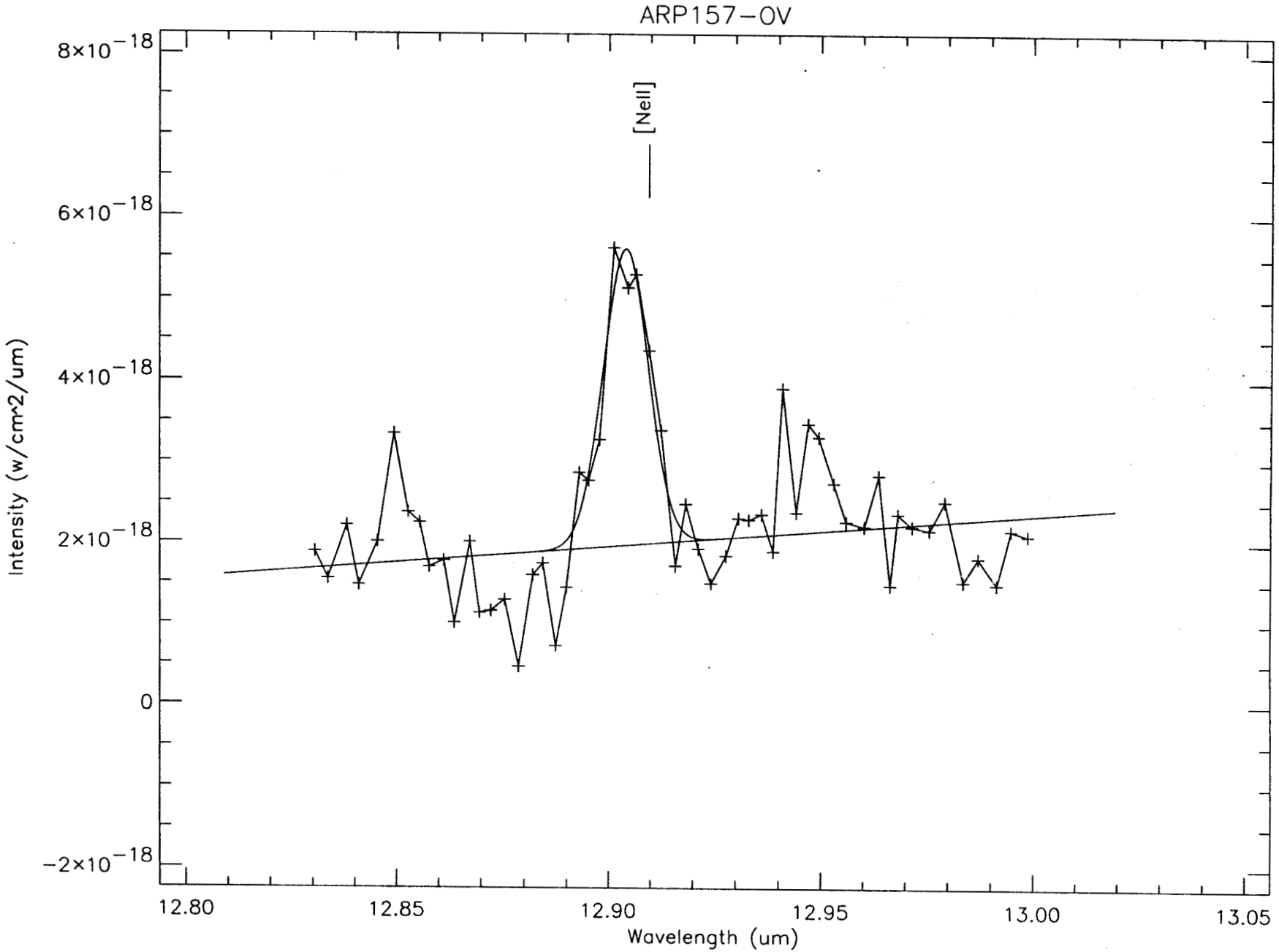
ARP157−OV
[NeII]
8×10−18
6×10−18
4×10−18
2×10−18
0
−2×10−18
Intensity (w/cm^2/um)
12.80
12.85
12.90
12.95
13.00
13.05
Wavelength (um)

Fig. 7